

Primary Sequence That Determines the Functional Overlap between Mitochondrial Heat Shock Protein 70 Ssc1 and Ssc3 of *Saccharomyces cerevisiae*^{*§}

Received for publication, October 25, 2010, and in revised form, March 15, 2011. Published, JBC Papers in Press, April 7, 2011, DOI 10.1074/jbc.M110.197434

Gautam Pareek, Madhuja Samaddar, and Patrick D'Silva¹

From the Department of Biochemistry, Indian Institute of Science, Bangalore 560012, Karnataka, India

The evolutionary diversity of the *HSP70* gene family at the genetic level has generated complex structural variations leading to altered functional specificity and mode of regulation in different cellular compartments. By utilizing *Saccharomyces cerevisiae* as a model system for better understanding the global functional cooperativity between Hsp70 paralogs, we have dissected the differences in functional properties at the biochemical level between mitochondrial heat shock protein 70 (mtHsp70) Ssc1 and an uncharacterized Ssc3 paralog. Based on the evolutionary origin of Ssc3 and a high degree of sequence homology with Ssc1, it has been proposed that both have a close functional overlap in the mitochondrial matrix. Surprisingly, our results demonstrate that there is no functional cross-talk between Ssc1 and Ssc3 paralogs. The lack of *in vivo* functional overlap is due to altered conformation and significant lower stability associated with Ssc3. The substrate-binding domain of Ssc3 showed poor affinity toward mitochondrial client proteins and Tim44 due to the open conformation in ADP-bound state. In addition to that, the nucleotide-binding domain of Ssc3 showed an altered regulation by the Mge1 co-chaperone due to a high degree of conformational plasticity, which strongly promotes aggregation. Besides, Ssc3 possesses a dysfunctional inter-domain interface thus rendering it unable to perform functions similar to generic Hsp70s. Moreover, we have identified the critical amino acid sequence of Ssc1 and Ssc3 that can “make or break” mtHsp70 chaperone function. Together, our analysis provides the first evidence to show that the nucleotide-binding domain of mtHsp70s plays a critical role in determining the functional specificity among paralogs and orthologs across kingdoms.

Heat shock proteins belonging to 70-kDa class (Hsp70s)² are implicated in a broad spectrum of cellular functions including

de novo protein folding, protein translocation across membranes, protein degradation, and regulation of the heat shock response (1–4). They are members of the *HSP70* multigene superfamily and ubiquitously expressed in different cellular compartments including, lumen of endoplasmic reticulum, mitochondrial matrix, and cytosol. There are several types of Hsp70s reported across species and usually they are present in 1 to 2 copies per cellular compartment with a distinct cellular function. Typically, Hsp70s comprise two functional domains: a highly conserved, N-terminal nucleotide-binding domain (NBD) and somewhat less conserved C-terminal substrate-binding domain (SBD). The biochemical activities of each domain are essential for general and specialized chaperone functions.

Hsp70s are an evolutionarily diverse group of proteins resulting from multiple gene duplication events across species (5, 6). The evolutionary significance of having multiple Hsp70 paralogs within the same cellular compartment at the functional level is not clearly established in higher eukaryotes. For example, the mitochondria of a well explored model organism such as *Saccharomyces cerevisiae* contain 3 Hsp70 paralogs: namely Ssc1, Ssq1, and Ssc3 (7). Ssc1 is the most abundant constitutively expressed multifunctional Hsp70 and is essential for the viability of yeast cells (8, 9). It plays a critical role in protein translocation across the mitochondrial inner membrane and folding of almost all pre-proteins targeted to the mitochondrial matrix compartment, thus maintaining protein homeostasis in mitochondria. For proper translocation function, Ssc1 is tethered to the translocation channel (Tim23-channel) as a core component of “import motor complex” via the peripheral membrane protein, Tim44 (10–13). During the translocation process, the presequence containing proteins interact with Ssc1 in an ATP-dependent manner and drive translocation of pre-proteins into the mitochondrial matrix in conjunction with other import motor components including J-class proteins, Pam18 (14–16), and Pam16 (17–19). Besides translocation function, Ssc1 together with Mdj1 (DnaJ homolog) and nucleotide exchange factor Mge1, plays a crucial role in folding of proteins that are imported into the mitochondrial matrix (20, 21).

The Ssq1 paralog is a highly specialized chaperone of the yeast mitochondrial matrix that shares 52% overall sequence identity with Ssc1. Ssq1 is not essential; however, cells lacking Ssq1 are cold sensitive as well as accumulate mitochondrial iron and are associated with reduced activities of enzymes containing Fe-S cluster. Ssq1 forms the core of the essential cellular machinery devoted to biogenesis of Fe-S clusters in the mito-

* This work was supported by Wellcome Trust International Senior Research Fellowship WT081643MA in Biomedical Science (to P. D.) and Council of Scientific and Industrial Research fellowships (to G. P. and M. S.).

§ Author's Choice—Final version full access.

§ The on-line version of this article (available at <http://www.jbc.org>) contains supplemental Figs. S1–S8 and Tables S1–S5.

¹ To whom correspondence should be addressed: C.V. Raman Ave., Bangalore 560012, Karnataka, India. Tel.: 91-080-22932821; Fax: 91-080-23600814; E-mail: patrick@biochem.iisc.ernet.in.

² The abbreviations used are: Hsp70, heat shock protein 70; mtHsp70, mitochondrial heat shock protein 70; NBD, nucleotide-binding domain; SBD, substrate-binding domain; TIM, translocase of the inner membrane; Hep1, human escort protein 1; F-P5, fluorescein-labeled P5; GPD, glyceraldehyde-3-phosphate dehydrogenase; TEF, translation elongation factor 1 α .

Comparative Analysis of Divergent Yeast mtHsp70 Paralogs

chondrial matrix. The yeast cells deleted for *SSQ1* can be partially rescued phenotypically by overexpressing *SSC1* indicating that both have overlapping functions at least in the Fe-S cluster assembly formation in fungi (22). Interestingly, however, specialized chaperones such as *Ssq1* by itself cannot substitute for the essential generic functions of mtHsp70 in yeast.

The *Ssc3* paralog is a minor Hsp70 of the yeast mitochondrial matrix that shares 82% sequence identity and overall 91% sequence similarity with *Ssc1*. *Ssc3* is conserved only among a lower subset of fungi believed to originate from duplication of *Ssc1* in fungal lineage (23). Under normal growth conditions, *Ssc3* expresses at ~500-fold lower levels than *Ssc1* (24, 25). Although *Ssc3* shares a very high degree of sequence homology with *Ssc1*, its cellular function is so far unknown. Based on the high sequence identity between *Ssc1* and *Ssc3* paralogs, it has been proposed that *Ssc3* may share common chaperone functions with *Ssc1* (26). However, due to sequence divergence in both domains of *Ssc3*, whether it retains a substantial functional overlap with *Ssc1* in the yeast mitochondrial matrix has not been investigated.

From our results, it is evident that there is no functional cross-talk between the highly identical Hsp70 paralogs *Ssc1* and *Ssc3* in the yeast mitochondrial matrix. The amino acid sequence divergence at critical positions in NBD and SBD of *Ssc3* leads to alteration in the biochemical properties of both domains at the functional level. *Ssc3* exhibited overall very weak affinity toward mitochondrial pre-sequence containing proteins, altered regulation with co-chaperones, especially *Mge1*, and defects in interaction with the Tim23-channel tethering protein, *Tim44*. Besides, the positioning of the linker region in *Ssc3* is considerably altered such that there is complete loss of inter-domain communication between the N- and C-terminal domains as well as overall significantly reduced thermal stability associated with the protein. Additionally, our detailed analysis at the level of the primary amino acid sequence has revealed the role of specific key amino acid residues in regulating the conformational differences between *Ssc3* and *Ssc1*. Based on our investigation, we hypothesize that *Ssc3* belongs to an “atypical Hsp70 class” and is functionally incompatible in assisting the *de novo* folding as well as translocation of pre-proteins in the mitochondrial matrix as in comparison to generic Hsp70, *Ssc1*.

EXPERIMENTAL PROCEDURES

Plasmid Construction and Yeast Strains—The wild type *SSC1*, *SSC3*, and all chimeric plasmid constructs were cloned under control of the *TEF/GPD* promoter either in a 2 μ plasmid pRS423 (*HIS*) or centromeric plasmid pRS413 (*HIS*) as described (supplemental Table S1). For solubilization of wild type *Ssc1*, *Ssc3*, and their respective NBD fragments with the linker region in the bacterial system, the corresponding coding sequences were cloned in pRSFDuet-1 vector along with the yeast Hep1 as described (supplemental Table S1). The DNA fragments corresponding to the SBD of *Ssc3*(415–644) and *Ssc1*(418–654), and full-length *Tim44*(43–431) with the TEV protease cleavable N terminus His₆ tag were cloned in pET vectors as described (supplemental Table S1). For bacterial expression of *Mge1*, Hep1, Pam18, and Pam16 proteins, the

corresponding coding nucleotide sequences were cloned in pRSFDuet-1 and pET vectors as described (supplemental Table S1). Point mutants of *Ssc1* and *Ssc3* were generated by QuikChange site-directed mutagenesis using high fidelity *Pfu* Turbo DNA Polymerase from Stratagene (supplemental Table S1). All clones were verified by DNA sequencing carried out at Eurofins Inc. All clones used for purification and *in vitro* experimental analysis were devoid of mitochondrial leader sequence based on the reported mature forms.

The yeast haploid strain *PJ53-52C* used in this study was a kind gift from Prof. E. A. Craig. The haploid *ssc3Δ* deletion and corresponding wild type (*BY4741*) yeast strains were obtained from Open Biosystems. For growth complementation analysis, the haploid *Δssc1* strain was transformed with a suitable plasmid carrying *SSC3* or various chimeric constructs under control of either *TEF* or *GPD* promoters. The transformants were selected on histidine omission plates. The transformants (His⁺) were then counter-selected on medium containing 5-fluoroorotic acid. The viable yeast cells were recovered on rich medium and subjected for drop test analysis using YPD and histidine omission plates to confirm the growth phenotypes. The genotypes of all the strains used for the analysis are summarized under supplemental Table S2.

Protein Expression, Solubility, and Purification Analysis—For solubility analysis of *Ssc1*, *Ssc3*, and their respective NBD fragments containing linker region, coexpression was carried out with yeast Hep1 in the *Escherichia coli* BL21(DE3) strain by allowing growth at specified temperatures (20, 30, 34, and 37 °C) to an *A*₆₀₀ of 0.8, followed by induction using 1 mM isopropyl 1-thio-β-D-galactopyranoside for 8 h. Cells were harvested by centrifugation and then lysed in buffer C (20 mM Hepes-KOH, pH 7.5, 150 mM KCl, 20 mM imidazole, 10% glycerol) containing 2.5 mM magnesium acetate, 0.2 mg/ml of lysozyme and protease inhibitor mixture, followed by incubation at 4 °C for 1 h. The samples were gently lysed with 0.2% deoxycholate followed by DNase I (10 µg/ml) treatment for 15 min at 4 °C. The mixtures were further lysed by sonicating 3 times (15 s) at 25% amplitude using an Ultrasonic processor with 2-min intervals on ice. The cell lysates were clarified by centrifuging at 28,000 × g for 30 min at 4 °C. The supernatant and pellet fractions were dissolved in SDS sample buffer and analyzed on 12.5% SDS-PAGE.

The purification of His-tagged *Ssc1* and *Ssc3* proteins were performed using similar protocols as previously described (27). Briefly, the *E. coli* BL21(DE3) cells transformed with the pRSFDuet-1 plasmid containing either *SSC1* or *SSC3* were grown at 30 and 20 °C, respectively, to an *A*₆₀₀ of 0.8, followed by induction using 1 mM isopropyl 1-thio-β-D-galactopyranoside for 8 h. Cell lysates were prepared by lysozyme treatment and the sonication method as described above. After centrifugation, the soluble supernatant was incubated with nickel-nitrilotriacetic acid-Sepharose for 2 h at 4 °C to allow binding. Unbound proteins and nonspecific contaminants were removed by multiple washes of buffer C alone followed by sequential single washes of buffer D (buffer C + 0.05% Triton X-100), buffer E (buffer C + 1 mM ATP, 10 mM MgCl₂), buffer F (buffer C + 1 M KCl), and buffer G (buffer C + 40 mM imidazole). Finally the bound proteins were eluted with buffer C containing 250 mM imidazole

and the samples were dialyzed against appropriate buffers for use in particular experiments. The nucleotide-free preparations of Ssc1 and Ssc3 were carried out according to published protocols (28). All the proteins including mutants, deletions, SBD, or NBD fragments of Ssc1 and Ssc3 were purified similar to the wild type protein, unless otherwise specified.

The His-tagged purification of proteins such as Mge1 and Mdj1 (29), Hep1 (30), Pam18 (31), and Tim44 (32) were carried out using previously published protocols. Greater than 95% purity was obtained for the preparations of mtHsp70s and its variants, Mdj1, Pam18, Mge1, Hep1, and Tim44 as analyzed on SDS-PAGE ([supplemental Fig. S1](#)).

Intrinsic Fluorescence and Anisotropy Peptide Binding Assay—Intrinsic fluorescence measurements were performed using a JASCO spectrofluorometer (6300) at a fixed excitation wavelength of 290 nm and emission spectra were recorded from 300 to 400 nm using 2.5-nm slit width.

Peptide binding analysis with fluorescein-labeled P5 (F-P5) peptide (CALLSAPRR) and Isu peptide (LSLPPVKLHC) in ADP-bound and ATP-bound states was performed as described previously with minor modifications (33, 34). Briefly, increasing concentrations of Ssc1, Ssc3 were incubated with 25 nM F-P5 at 20 °C in buffer A for 1 h. After binding reached equilibrium, the anisotropy measurements were recorded on a Beacon-2000 fluorescence polarization system (Panvera, Madison, WI) using excitation at 490 nm and emission at 535 nm. The normalized data were fitted to a one-site binding hyperbola equation using GraphPad Prism 5.0 to calculate the equilibrium dissociation constant (K_d). The k_{off} measurements in ADP-bound state were done as per previously published protocols (34) and the data were fitted to one phase exponential dissociation equation using GraphPad Prism 5.0. For determination of the ATP-dependent peptide release, 250 μM ATP was added to the preformed Hsp70·F-P5 complex, and decrease in fluorescence anisotropic values were recorded at the 12-s intervals. The normalized millipolarization values were plotted against time and fitted to a one-phase exponential dissociation equation.

Partial Tryptic Digestion Analysis—Partial tryptic digestion of different proteins was performed similar to protocols used for *E. coli* DnaK (35). Briefly, Ssc1, Ssc3, or fragments (~5 μg) were incubated in buffer B (40 mM Tris-HCl (pH 7.5), 8 mM magnesium acetate, 20 mM NaCl, 20 mM KCl, 0.3 mM EDTA, and 2 mM DTT) at 15 °C for 30 min. The proteolytic digestion was initiated by addition of 0.1 μg of trypsin (trypsin type 1 from bovine pancreas, Sigma) to the reaction mixture. The samples were taken out at various intervals as indicated, and analyzed on SDS-PAGE followed by Coomassie Blue staining. For protein microsequencing, the bands were electroblotted onto polyvinylidene difluoride membrane and the bands of interests were excised from the membrane followed by N-terminal sequencing using a Procise protein sequencer from Applied Biosystems.

CD Measurements and Thermal Aggregation Assay—Far UV CD spectra were recorded on a JASCO-810 spectropolarimeter equipped with a temperature controlling system. The spectra were recorded from 190 to 260-nm wavelengths with 20 mdeg sensitivity at a scan speed of 50 nm/min and a bandwidth of 2

nm. The time constant was 4 s and each spectrum an average of 10 scans. The protein concentration used was 1.0 μM in 10 mM sodium phosphate (pH 7.5) and the cuvette path length was 2 mm. The thermal unfolding was measured at a fixed wavelength of 222 nm with increasing temperature ranging from 5 to 90 °C at a scanning rate of 60 °C h⁻¹. The spectra were measured in mdeg, corrected for buffer effects, and expressed as mean residue ellipticity (θ).

For thermal aggregation experiments, aliquots of 0.5 mg/ml of Ssc1 and Ssc3 in buffer A containing 5% glycerol were incubated at different temperatures as indicated for 30 min followed by a 10-min centrifugation at 28,000 × g. The pellet and supernatant fractions were analyzed on 12.5% SDS-PAGE followed by staining with Coomassie Brilliant Blue.

Other Methods—Single turnover ATPase assays (36), calcofluor white hypersensitivity test (37), *in vivo* precursor accumulation analysis (38), rhodanese aggregation assays, GST pull-down analysis, yeast mitochondria isolation, and fractionation were done using standard protocols as previously described unless otherwise specified (27, 39). The antisera used for immunodecoration against yeast-specific proteins such as Hsp60, Mge1, Tim23, Ssc1, and Ydj1 were raised in rabbits as previously reported (31). The HA-Ssc3 protein was detected using anti-HA mouse 12CA5 (Roche Applied Science). Immunoblot analysis was carried out by using the ECL system (Pierce) according to the manufacturer's instructions.

RESULTS

Ssc3 Protein Lacks Functional Cooperativity with Generic Hsp70 Ssc1 in Yeast Mitochondria—Sequence alignment of Ssc3 and Ssc1 displays overall 82% homology and 91% similarity at the protein level ([supplemental Fig. S2](#)). Based on the high degree of sequence conservation between Ssc3 and Ssc1 and their similar destination raised the possibility of a functional overlap at the biochemical level. However, the biological function of Ssc3 is yet to be rigorously established in *S. cerevisiae* as well as in other fungal species. In a genome-wide analysis, *SSC3(ECM10)* was identified as a candidate whose deletion showed increased sensitivity to the cell wall perturbing agent, calcofluor white (40). However, involvement of this mitochondrial chaperone in cell wall biogenesis remained elusive so far. To validate this observation, we performed a calcofluor white hypersensitivity test at different concentrations using rich and minimal medium. Interestingly, *ssc3Δ* cells showed no obvious growth defects indicating that its direct involvement as a chaperone in cell wall biogenesis may be limited ([supplemental Fig. S3](#)).

To investigate a possible functional overlap between Ssc3 and Ssc1 paralogs, we have conducted *in vivo* growth complementation analysis of *ssc1Δ* cells by expressing Ssc3 under various constitutive promoters using a high copy 2μ plasmid. We observed that Ssc3 does not support the growth of *ssc1Δ* cells when expressed under the endogenous promoter of Ssc1 using high copy plasmid, consistent with previous reports (24) (data not shown). Equally, Ssc3 failed to support the *ssc1* null mutation when overexpressed under control of stronger constitutive promoters such as *TEF* or *GPD* using 2μ plasmid ([supplemental Fig. S4A](#)). To ascertain that under different overexpression con-

Comparative Analysis of Divergent Yeast mtHsp70 Paralogs

ditions Ssc3 was efficiently imported into the matrix, we have tested the protein levels in the isolated mitochondria by immunoblotting analysis using HA-specific antibodies. As indicated under supplemental Fig. S4B an increased level of Ssc3 overexpression was observed in mitochondria based on promoter strength as in comparison to its undetectable endogenous protein levels. To confirm further whether overexpression of Ssc3 can partially compensate the phenotypic defects associated with the *SSC1* mutation, we have utilized a temperature-sensitive (Ts) *ssc1-2* mutant carrying a single amino acid substitution in the substrate-binding domain (P442S) (41). Even at higher expression levels, Ssc3 failed to rescue the temperature-sensitive growth phenotype as well as the import defect of the *ssc1-2* mutant as tested by Hsp60 precursor accumulation analysis (supplemental Fig. S4, C and D). Intriguingly, these results strongly argue against a possible functional overlap between Ssc3 and Ssc1 paralogs despite having a high degree of sequence identity between them. To dissect out the molecular basis of functional variability between these two highly identical paralogs, we have assessed the differences at the structural level that are attributable to changes in biochemical properties of Ssc3 in comparison to Ssc1.

Ssc3 Possesses Significantly Weaker Affinity for Mitochondrial Client Proteins—Yeast mitochondrial Hsp70s, Ssc1 and Ssc3, share 97% similarity in the β -sandwich subdomain and 91% similarity in variable helical lid region (supplemental Fig. S2). Based on this high sequence conservation in SBD, it is tempting to speculate that both chaperones might have overlapping substrate specificities. To explore the substrate binding properties of Ssc3, we have utilized the fluorescence anisotropy-based peptide binding assay. We have utilized a generic Hsp70 model peptide, P5 (CALLLSAPRR), derived from a portion of the mitochondrial targeting sequence of aspartate aminotransferase from chicken. The P5 peptide was labeled with fluorescein fluorophore covalently attached to the cysteine residue. The fluorescence anisotropy assay measures the relative changes in tumbling rates of fluorescent-labeled peptides upon binding of Hsp70 in solution.

Ssc3 yielded a very high dissociation constant (K_d of $30.13 \pm 2.131 \mu\text{M}$) for the P5 peptide binding (Fig. 1A). Strikingly, the K_d of Ssc3 for P5 peptide was 100-fold higher than the Ssc1 paralog (K_d of $0.231 \pm 0.014 \mu\text{M}$) in the ADP-bound state (Fig. 1A). Moreover, this affinity of Ssc3 in the ADP-bound state was within or closer to the reported K_d values for P5 peptide binding in the ATP-bound state of Ssc1 (34). Interestingly, when P5 binding was analyzed in the ATP-bound state, both Ssc3 and Ssc1 showed very similar affinity with K_d of 26.30 ± 1.332 and $30.86 \pm 2.604 \mu\text{M}$, respectively (Fig. 1B). These observations reveal a possible open conformation associated with SBD of Ssc3 even in the ADP-bound state. To gain further insight into the substrate binding mechanism of Ssc3, we characterized the kinetics of P5 peptide binding using anisotropy measurements. Importantly, Ssc3 showed a very high dissociation rate (k_{off} of $0.244 \pm 0.004 \text{ s}^{-1}$) as analyzed by addition of a 1000-fold excess of unlabeled P5 into the preformed Ssc3-F-P5 complex followed by anisotropy measurements as a function of time (Fig. 1C). Interestingly, this k_{off} was 80-fold faster than the dissociation rate of Ssc1 (k_{off} of 0.003 s^{-1}) for P5 peptide in the ADP-bound

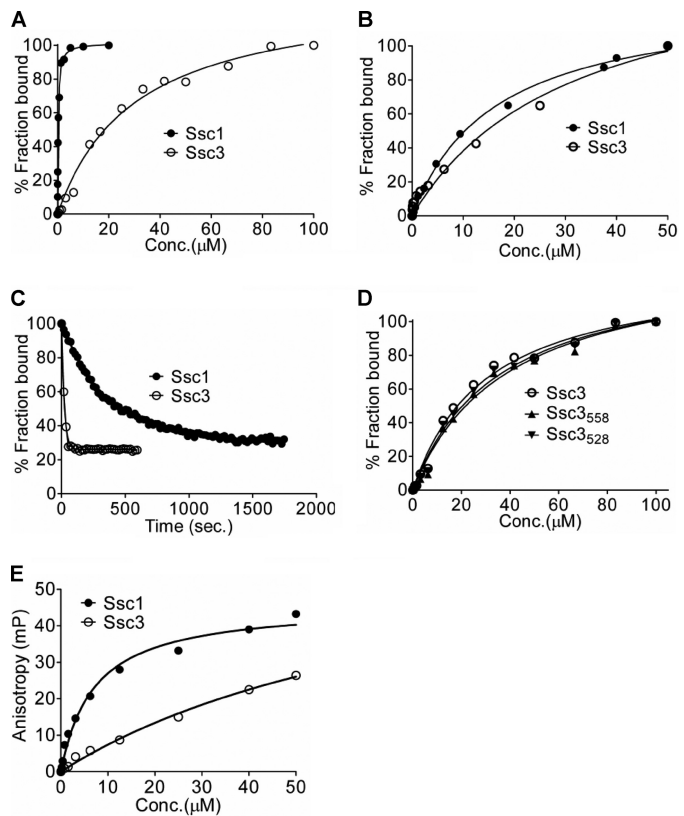


FIGURE 1. Fluorescence anisotropy assay of peptide binding for Ssc3, Ssc1, and deletion mutants. *A*, 25 nm fluorescein-labeled P5 (F-P5) peptide was incubated in the presence of the indicated concentrations of preformed wild type yeast Ssc1-ADP and Ssc3-ADP proteins. Fluorescence anisotropy measurements were recorded as described under “Experimental Procedures.” *B*, increasing concentrations of preformed Ssc1-ATP or Ssc3-ATP complexes were incubated with 25 nm F-P5 and the binding was monitored by measuring the anisotropy kinetically at 12-s intervals. After binding reached saturation (within 2 min), the values were fitted to one-site binding equation to calculate the equilibrium constant in the ATP state. *C*, 1000-fold excess of unlabeled P5 was added to the preformed Ssc1 or Ssc3-F-P5 complex in the ADP-bound state and loss of fluorescence anisotropy of bound F-P5 was monitored at 12-s intervals. The millipolarization values were normalized after subtracting the background and fitted to a one-phase exponential dissociation equation to calculate k_{off} . *D*, increasing indicated concentrations of Ssc3 and its deletion mutants (Ssc3₅₅₈ and Ssc3₅₂₈) incubated with 25 nm F-P5 at 15 °C. After binding reached equilibrium, the fluorescence anisotropy were recorded and fitted to a one-site binding hyperbola equation to calculate the K_d . *E*, fluorescence anisotropy measurements were taken using fluorescein-labeled Ius1 peptide (F-Ius1) for Ssc1 and Ssc3 proteins as described above.

state, further supporting an open conformation of the SBD of Ssc3 (Fig. 1C).

In generic Hsp70s, such as *E. coli* DnaK and yeast Ssc1, deletion of the helical lid region dramatically reduces the substrate binding affinity by significantly enhancing the dissociation rate for peptides (33, 42–44). To validate whether the apparent lower affinity for peptide binding in Ssc3 is due to altered orientation of the helical lid over the peptide binding cleft, we have constructed two deletion mutants: 1) truncating at the hinge portion of helix B (Ssc3₅₅₈), and 2) removal of the complete helical lid region (Ssc3₅₂₈). Surprisingly, both the truncation mutants and wild type showed similar affinity toward P5 binding in ADP-bound state indicating that the helical lid region is not critical for regulating the substrate binding (Fig. 1D). Importantly, the helical lid not being tightly associated with the peptide binding cleft indicates a constitutively open conforma-

tion of the Ssc3 SBD similar to the ATP-bound state of generic Hsp70s, like DnaK and Ssc1.

The specialized Hsp70 paralog such as Ssq1 functions in iron-sulfur (Fe-S) cluster biogenesis in the mitochondrial matrix. This requires interaction with a "PVK tripeptide" motif of the Isu1 scaffold on which Fe-S clusters are assembled prior to transfer into recipient apoproteins (45). Previous biochemical analysis showed that both Ssc1 and Ssq1 can efficiently interact with "PVK" motif of Isu1, thus possessing an overlapping function in the Fe-S cluster formation (23). To assess the possible role of Ssc3 in Fe-S cluster biogenesis, we have analyzed interaction of the PVK motif containing the Isu1 peptide (LSLPPVKLHC), which is labeled with fluorescein to the cysteine residue at the C terminus. Previously, this assay has been utilized for quantitative interaction analysis between Isu1 and Ssc1/Ssq1 proteins. By anisotropic measurements we observed that Ssc3 displayed extremely poor affinity with $K_d > 90 \mu\text{M}$ toward the Isu1 peptide as in comparison to Ssc1 (K_d of $7.066 \pm 0.872 \mu\text{M}$) (Fig. 1E). This K_d was 40-fold lower than the intrinsic affinity of the Ssq1 paralog for Isu1 binding, indicating that the function of Ssc3 is rather limited in Fe-S cluster formation in the mitochondrial matrix (46). These observations are in agreement with previously reported *in vivo* complementation analysis (23).

As an additional functional parameter, we have assessed the ability of yeast mtHsp70s in preventing the aggregation of client proteins using rhodanese as a model substrate. As shown under supplemental Fig. S5A, at 5-fold molar excess of Ssc1, ~60% protection was observed with denatured rhodanese as compared with the BSA control. However, under similar conditions Ssc3 failed to prevent the aggregation of denatured rhodanese (supplemental Fig. S5A), suggesting that due to poor substrate binding affinity, Ssc3 is unable to perform the functions similar to generic Hsp70s like Ssc1. Additionally, purified SBD of Ssc3 in contrast to the Ssc1 SBD failed to show any detectable interaction with the membrane anchor protein Tim44 as analyzed by a nickel-nitrilotriacetic acid pulldown assay, rendering the possible involvement of this chaperone in protein import highly unlikely (supplemental Fig. S5B). Overall, we conclude that even though Ssc3 and Ssc1 have very high sequence conservation at the amino acid level in SBD, there are significant conformational differences existing between them, which contribute for the differences in interaction with mitochondrial client protein substrates as well as with the membrane anchor protein Tim44.

SBD of Ssc3 Is Less Stable Due to Open Conformation as Compared with Generic Hsp70s—To gain further insight into the conformational differences existing between Ssc1 and Ssc3; we have utilized two different *in vitro* experimental approaches. As a first approach we have performed limited proteolysis previously being used for inferring the presence of stable sub-domains and to monitor nucleotide-dependent conformational changes in various Hsp70 proteins. In the case of bacterial Hsp70 DnaK, tryptic digestion in the ADP-bound state leads to accumulation of stable SBD fragment (35, 47). Interestingly, a similar cleavage pattern was observed in the case of Ssc1, where the ADP-bound state showed generation of a stable ~26-kDa SBD fragment upon a time course trypsin cleavage (Fig. 2A, left

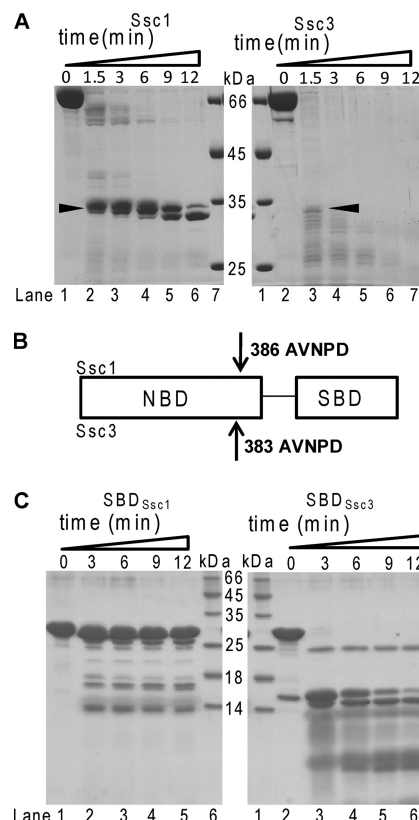


FIGURE 2. Proteolytic susceptibility of Ssc1, Ssc3, and their respective SBDs. *A*, 5 μg of Ssc1 (left panel) or Ssc3 (right panel) protein was preincubated in cleavage buffer for 30 min at 15 °C. The proteolysis was initiated by addition of 0.1 μg (1:50, w/w) of trypsin. The reaction was stopped at the indicated time intervals using 2 mM PMSF. The samples were boiled using SDS sample buffer and analyzed on SDS-PAGE followed by Coomassie dye staining. The highlighted bands (indicated as ▲) were electroblotted and subjected to microsequencing. *B*, schematic representation of the domain structures of Ssc1 and Ssc3. The amino acid positions of the trypsin cleavage site in Ssc1 (upper) and Ssc3 (lower) are indicated. *C*, 5 μg of SBDs of Ssc1 (left panel) and Ssc3 (right panel) were subjected to partial tryptic digestion as mentioned in *A*.

panel, lanes 2–7). The cleavage site was identified at amino acid position 386 by N-terminal microsequencing (Fig. 2B). However, in case of Ssc3, a band corresponding to SBD disappeared in the subsequent time course of tryptic digestion (Fig. 2A, right panel, lanes 2–7). Therefore it provides strong evidence in favor of an ATP-bound state-like open conformation associated with SBD of the Ssc3 protein. Additionally, when purified SBDs of both Hsp70s were subjected for tryptic digestion, SBD of Ssc3 was highly susceptible to proteolytic digestion (Fig. 2C, right panel, lanes 2–6) indicating an open conformational state of this domain, whereas purified SBD of Ssc1 was found to be highly resistant due to its compact structure (Fig. 2C, left panel, lanes 2–6), similar to generic Hsp70-like *E. coli* DnaK (35).

As a second approach, we have employed circular dichroism to assess the stability of Ssc3 and Ssc1 upon thermal denaturation. As indicated in Fig. 3A, left panel, a comparison of shapes and ellipticity values suggests that both proteins harbor similar secondary structural content. To analyze whether the thermal stability of Ssc3 was different from Ssc1, the ellipticity at 222 nm was measured as a function of temperature. Similar to other Hsp70s like DnaK, wild type Ssc1 showed two different thermal transitions of 41.3 ± 0.3 °C for NBD and 68.5 ± 0.5 °C for SBD

Comparative Analysis of Divergent Yeast mtHsp70 Paralogs

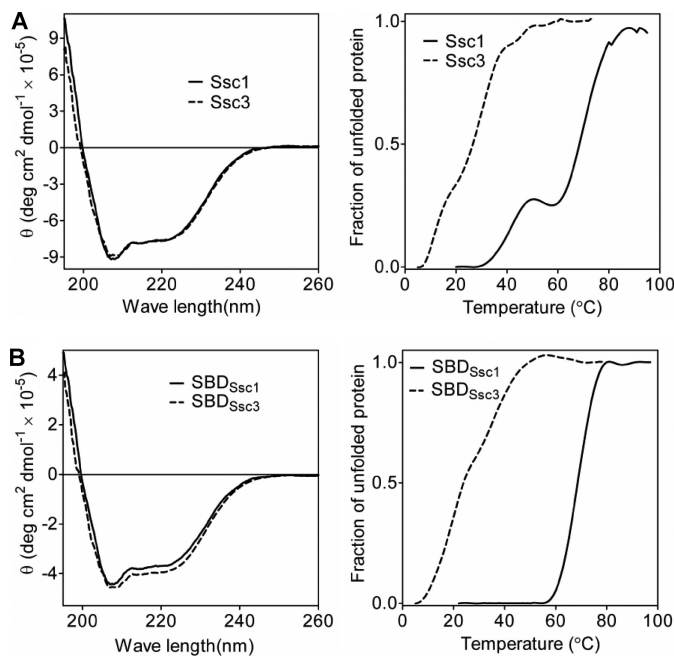


FIGURE 3. Measurement of thermal stability of Ssc1, Ssc3, and their respective SBDs using CD. *A*, far UV CD spectra of Ssc1 (solid line) and Ssc3 (dashed line) in 10 mM phosphate buffer (pH 7.5) was recorded at 10 °C (left panel). The thermal melting curves for Ssc1 (solid line) and Ssc3 (dashed line) were obtained by monitoring the ellipticity at 222 nm as a function of temperature (right panel). *B*, far UV CD spectra of SBD_{Ssc1} (solid line) and SBD_{Ssc3} (dashed line) (left panel) and thermal melting curves for SBD_{Ssc1} (solid line) and SBD_{Ssc3} (dashed line) (right panel) were recorded as described in *A*.

(Fig. 3*A*, right panel, solid line) (48, 49). On the other hand, the thermal melting curve of Ssc3 differs considerably and showed a significant decrease in thermal stability (Fig. 3*A*, right panel, dashed line). Surprisingly, Ssc3 lacked the presence of two different transitions in contrast to other generic Hsp70s. The thermal unfolding transition was found to be unexpectedly low at 29.2 ± 0.2 °C for Ssc3. We reasoned that the apparent lack of two transitions in Ssc3 may be due to close overlap in the thermal unfolding transitions of SBD and NBD. To validate our observation we have analyzed thermal stability of the purified SBDs from Ssc3 and Ssc1 using CD measurements. The overall secondary structure and shape of the CD spectrum of SBD of Ssc3 were found similar to the SBD of Ssc1 (Fig. 3*B*, left panel). However, the rate of thermal unfolding of SBD of Ssc3 was found to be significantly faster than SBD of Ssc1. Typically, the SBDs alone of generic Hsp70s show the thermal transition temperature (T_m) for 50% unfolding at around 68–70 °C. The Ssc3 SBD showed significantly lower T_m of 27.1 ± 0.1 °C as compared with the SBD of Ssc1 (T_m of 68.8 ± 0.3 °C) (Fig. 3*B*, right panel). Taken together, our observations suggest that subtle amino acid variations in the SBD of Ssc3 during evolution significantly enhanced the conformational plasticity of the C-terminal domain, therefore, rendering it unable to function similar to generic Hsp70 under *in vivo* conditions.

Critical Amino Acid Sequence Required for the Regulation of Substrate Binding Affinity in Yeast mtHsp70 Paralogs—Our experimental analysis has revealed that the SBD of Ssc3 is associated with a constitutively open conformation. To uncover the amino acid sequence that determines the poor affinity of Ssc3 for substrates, we have generated a chimeric protein, SBD_{Ssc1}–

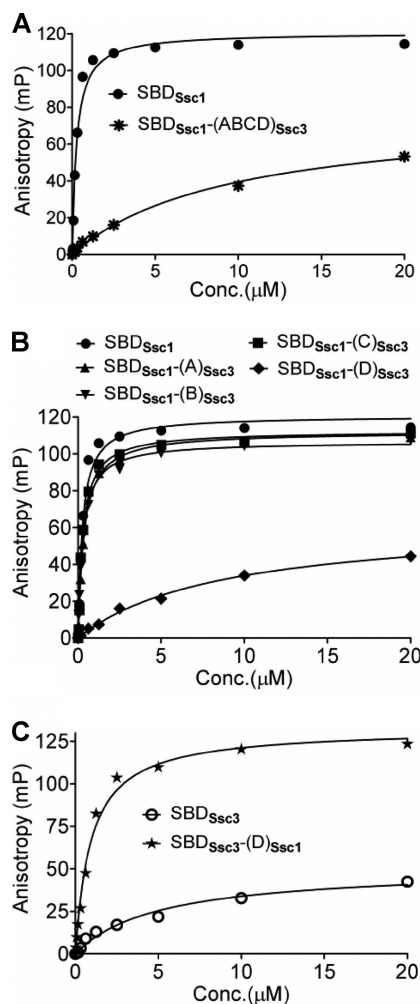


FIGURE 4. Fluorescence anisotropy assay of peptide binding for SBD_{Ssc1}, SBD_{Ssc3}, and chimeric proteins. Fluorescence anisotropy measurements were taken using fluorescein-labeled P5 peptide (F-P5) as described in the legend to Fig. 1. *A*, SBD_{Ssc1}-(ABCD)_{Ssc3} chimera in which the variable domain of SBD_{Ssc1} is replaced with that of SBD_{Ssc3}. *B*, SBD_{Ssc1}-(A)_{Ssc3}, SBD_{Ssc1}-(B)_{Ssc3}, SBD_{Ssc1}-(C)_{Ssc3}, and SBD_{Ssc1}-(D)_{Ssc3} where the A-, B-, C-, and D-helix of SBD_{Ssc1} are individually replaced with that of SBD_{Ssc3}, respectively. *C*, SBD_{Ssc3}-(D)_{Ssc1} in which the D helix of SBD_{Ssc3} is replaced with that of SBD_{Ssc1}.

(ABCD)_{Ssc3}, in which the variable domain of the SBD of Ssc1 is replaced with Ssc3. This chimeric protein showed 86-fold reduction in P5-binding (K_d of 22.724 ± 1.008 μM) as compared with wild type (K_d of 0.264 ± 0.041 μM), highlighting that the variable region of the SBD in Ssc3 is responsible for poor affinity toward mitochondrial client protein binding (Fig. 4*A* and supplemental Table S3). Similar to generic Hsp70s, the variable domain of Ssc3 consists of five different helices namely: A-, B-, C-, D-, and E-helix. Of these helices, the amino acid sequence of the E-helix is totally conserved with Ssc1 (supplemental Fig. S2). On the other hand, substantial amino acid changes have occurred at various positions within A-, B-, C-, and D-helix of Ssc3. Therefore, to identify which helix plays a key role in determining the substrate binding affinity between Ssc3 and Ssc1, we have replaced helices from A to D of the SBD of Ssc1 with Ssc3 by generating 4 chimeric proteins namely, SBD_{Ssc1}-(A)_{Ssc3}, SBD_{Ssc1}-(B)_{Ssc3}, SBD_{Ssc1}-(C)_{Ssc3}, and SBD_{Ssc1}-(D)_{Ssc3}. Interestingly, we observed that swapping A-, B-, or C-helix showed similar P5 binding in comparison with the wild type SBD of

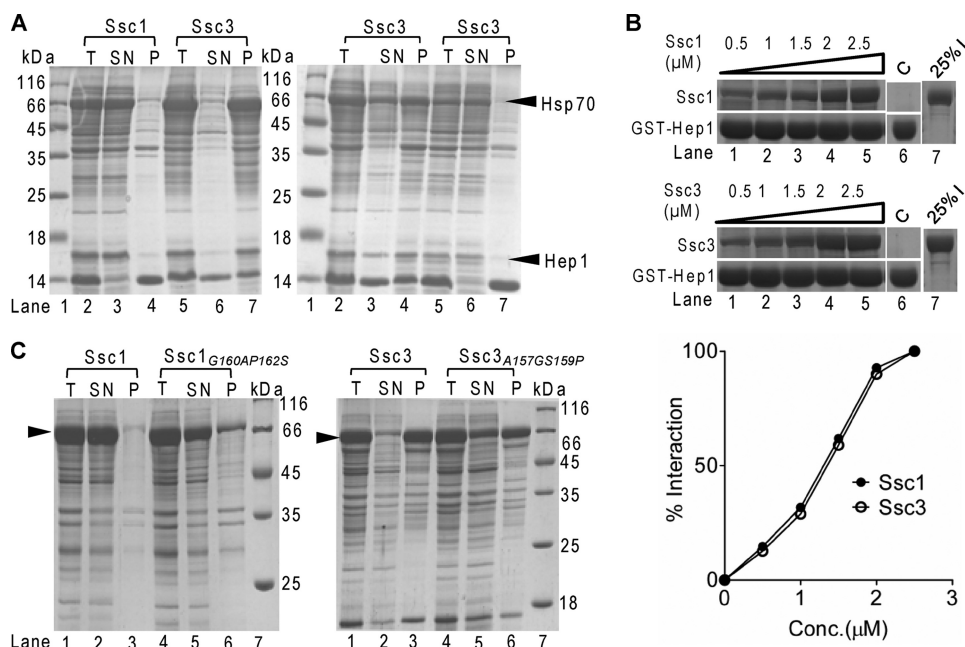


FIGURE 5. Solubility analysis of Ssc1, Ssc3, and their variants. *A*, full-length Ssc1 and Ssc3 were coexpressed with yeast Hep1 in *E. coli* cells grown at 37 °C (left panel) and 30 and 20 °C (right panel). Cells were harvested and lysed using lysozyme treatment followed by sonication. The crude lysates were centrifuged to separate the soluble supernatant fraction (SN) and insoluble pellet fraction (P). The samples were dissolved in SDS sample buffer and analyzed on SDS-PAGE followed by Coomassie dye staining. The crude lysates before centrifugation were used as positive loading control (7). The bands corresponds to Hsp70 (Ssc1 and Ssc3) and Hep1 are indicated. *B*, *in vitro* GST pulldown interaction between Ssc1 or Ssc3 and yeast Hep1 protein. Immobilized GST-Hep1 (1.5 μM) was incubated with increasing concentrations of Ssc1 and Ssc3 as indicated, in the absence of nucleotides. The bound proteins were analyzed by SDS-PAGE followed by Coomassie dye staining. GST alone was used as a negative control and 25% input (offered to the beads) was used as a loading control (top panel). The data were quantified by densitometric analysis using ImageQuant software (bottom panel). *C*, the expression and solubility analysis of Ssc1 mutant (Ssc1_{G160A,P162S}) (left panel, lanes 4–6) and Ssc3 mutant (Ssc3_{A157G,S159P}) (right panel, lanes 4–6) proteins were performed as described in *A*. The position of mtHsp70 is highlighted (indicated as ▲).

Ssc1 (Fig. 4*B* and supplemental Table S3). Strikingly, upon swapping the D-helix (from Ala-600 to Ser-623), a 78-fold reduction in P5 binding was observed for the SBD_{Ssc1}-(D)_{Ssc3} chimeric protein (Fig. 4*B* and supplemental Table S3), which was very much comparable with that of wild type SBD of Ssc3. Based on these observations, we hypothesize that the D-helix of mtHsp70s plays a crucial role in determining substrate binding affinity. Therefore, to convert the SBD of Ssc3 to make it similar to the SBD of generic Hsp70s in terms of peptide binding, we have generated a chimera SBD_{Ssc3}-(D)_{Ssc1} in which the D-helix of Ssc3 was replaced by Ssc1. Interestingly, the chimera SBD_{Ssc3}-(D)_{Ssc1} showed a significant improvement in P5-binding with K_d of 0.911 μM (\pm 0.087 μM) as compared with the wild type SBD of Ssc3 (Fig. 4*C* and supplemental Table S3). Therefore, our findings clearly highlight that the D-helix plays a critical role in determining the functional overlap between mtHsp70 paralogs as far as SBD is concerned.

NBD of Ssc3 Has Significantly Altered Conformation from Other mtHsp70s—In mitochondria, the Hep1 (Zim17) co-chaperone modulates the conformational status of Hsp70 thereby preventing their aggregation and maintaining the function of mitochondrial Hsp70 chaperones (50). Ssc3 when overexpressed under control of the endogenous Ssc1 promoter results in partial aggregation in mitochondria even in the presence of Hep1 (supplemental Fig. S6*A*). In contrast, Ssc1 and Ssq1 paralogs remain soluble upon overexpression in mitochondria (supplemental Fig. S6*A*). Similarly, mitochondrial Hsp70 family members aggregate upon overexpressing alone in *E. coli* cells. However, upon coexpression with Hep1, Hsp70s

such as Ssc1 remains soluble in *E. coli* cells at 37 °C (Fig. 5*A*, left panel, lanes 2–4). Interestingly, the solubility of Ssc3 was significantly lower as in comparison to Ssc1 upon coexpression at 37 °C (Fig. 5*A*, left panel, lanes 5–7). Our observations were consistent with previously reported results (39). Moreover, Ssc3 was partially soluble at 30 °C and recovered >95% in the supernatant fraction upon induction at 20 °C (Fig. 5*A*, right panel, lanes 2–7).

To investigate whether the tendency of Ssc3 to aggregate at 37 °C is due to its poor interaction with the co-chaperone Hep1, we have performed *in vitro* interaction analysis between Ssc3 and Hep1 using GST pulldown assay. Increasing concentrations of purified Ssc3 or Ssc1 proteins were incubated with the GST-bound Hep1 protein and subjected to pulldown analysis. As indicated in Fig. 5*B*, both Ssc3 and Ssc1 could interact efficiently with GST-Hep1 in the non-nucleotide state (Fig. 5*B*, lanes 1–5). Both Ssc3 and Ssc1 showed almost similar affinities (K_d of ~1.5 μM) for the Hep1 interaction. Our observations suggest that aggregation of Ssc3 is an intrinsic property of the protein rather than a defect in interaction with Hep1.

To validate our observation *in vitro*, we assessed the thermal stability of purified Ssc3 and Ssc1 at different temperature conditions to monitor the aggregation upon denaturation. At 25 °C, Ssc3 was stable and a negligible amount was found in the pellet fraction (supplemental Fig. S6*B*, bottom panel, lanes 1 and 2). However, at 30 °C, >50% and at 35 °C almost 100% of Ssc3 protein was aggregated into the pellet fraction (supplemental Fig. S6*B*, bottom panel, lanes 3–8). In contrast to Ssc3, under similar conditions, Ssc1 was very stable and a negligible

Comparative Analysis of Divergent Yeast mtHsp70 Paralogs

amount was found in the aggregated fraction ([supplemental Fig. S6B, top panel, lanes 1–8](#)).

To understand the driving force behind the aggregation of Ssc3, we expressed its individual domains, NBD and SBD in *E. coli*. The SBD of Ssc3 alone, when overexpressed remains soluble even in the absence of Hep1 similar to other Hsp70s (data not shown). Previously it has been reported that the NBD of mtHsp70s is one of the molecular determinants for low solubility upon expression in the bacterial system (51). Consistent with these results, we have also observed that the NBD of Ssc3 was insoluble upon coexpressing with Hep1 in contrast to the NBD of Ssc1 ([supplemental Fig. S6C, lanes 2–7](#)). However, the level of interaction of Ssc3 and Ssc1 NBDs with Hep1 was found comparable by GST pulldown analysis (data not shown). Therefore, we conclude that insolubility of the Ssc3 protein at higher temperatures is attributable to the overall stability and conformational flexibility associated with NBD acquired during evolution due to sequence variation as in comparison to generic Hsp70s.

To further probe the conformational differences associated with the NBD of Ssc3, we have subjected it to limited proteolysis using trypsin. As indicated under [supplemental Fig. S6D](#), the NBD of Ssc3 was extremely susceptible to trypsin cleavage in the ADP-bound state. However, similar to the isolated NBDs of other generic Hsp70s, such as DnaK, NBD of Ssc1 was found to be very stable against trypsin proteolytic cleavage (35) ([supplemental Fig. S6D](#)). These results clearly highlight possible conformational differences in NBD of Ssc3 in comparison to another mtHsp70, Ssc1.

The NBD of Ssc3 shares 87% sequence identity and 94% sequence similarity with Ssc1. During evolution, 52 amino acid substitutions have occurred in the NBD of Ssc3 as compared with the sequence of Ssc1. Of these, 24 amino acid substitutions are found to be canonical, whereas the remaining are non-canonical in nature. To identify the critical amino acids in NBD of Ssc3, which contribute to the altered function and aggregation property, we compared the primary sequence with other generic Hsp70s from different species including Ssc1, DnaK, and human mtHsp70. To make the NBD of Ssc1 similar to Ssc3, we have generated several point mutants of Ssc1 in which amino acid substitution was made with the corresponding identical amino acid from Ssc3 ([supplemental Table S4](#)). The Ssc1 mutants were analyzed for aggregation by coexpressing with Hep1. As shown earlier, wild type Ssc1 is completely soluble at 37 °C upon coexpression with Hep1 (Fig. 5C, *left panel, lanes 1–3*). Interestingly, few of the mutant proteins showed a variable degree of protein aggregation as compared with wild type ([supplemental Table S4](#)). Most notably, the double mutant G160A,P162S showed ~25–30% distribution in the pellet fraction (Fig. 5C, *left panel, lanes 4–6*, and [supplemental Table S4](#)). In bacterial DnaK, the corresponding amino acid residues (Gly-132 and Pro-134) are located in a turn that contributes to the interface of NBD with SBD, therefore possibly playing a critical role in regulating the Hsp70 function (52). To validate this hypothesis, we have introduced the mutations in Ssc3 at similar positions (A157G,S159P) using a corresponding sequence from Ssc1. Interestingly, the Ssc3_{A157G,S159P} mutant protein showed enhanced solubility upon overexpression in *E. coli* at 37 °C in

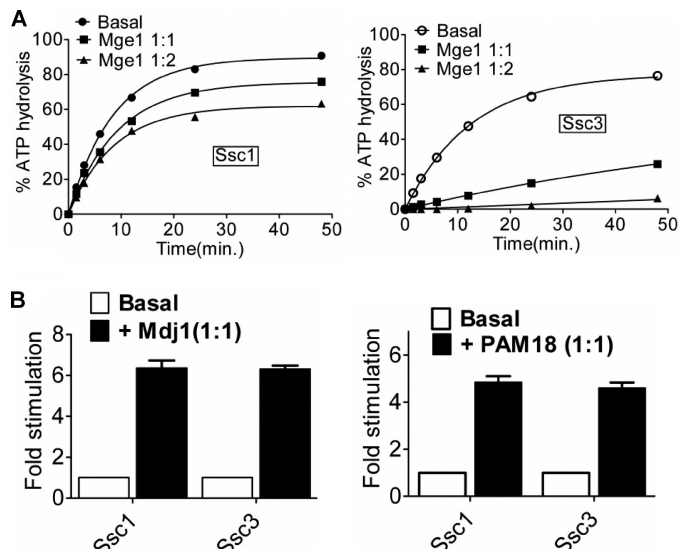


FIGURE 6. Probing the conformational differences between NBDs of Ssc1 and Ssc3 through co-chaperone interaction. *A*, the preformed radiolabeled Ssc1-ATP (left panel) and Ssc3-ATP (right panel) complexes (~0.5 μM) were incubated either in buffer A (20 mM Hepes-KOH, pH 7.5, containing 100 mM KCl, 10 mM magnesium acetate, 10% glycerol) alone or with the indicated ratios of Mge1, and *B*, the indicated ratios of Mdj1 (left panel) and Pam18 (right panel) at 25 °C. ATP hydrolysis was monitored as a function of time, and percentage of ATP to ADP conversion at various time intervals was plotted. Fold-stimulation was calculated by setting the intrinsic ATP hydrolysis rate as 1. Error bars are derived from two independent sets of experiments.

comparison to wild type Ssc3 (Fig. 5C, *right panel, lanes 1–6*, and [supplemental Table S4](#)). Based on these observations, we propose that amino acid residues corresponding to the 157th and 159th positions of NBD play a crucial role in maintaining the solubility and aggregation propensity of Ssc3. However, the decrease in solubility as observed for this double mutant is insufficient to account for the striking difference between Ssc1 and Ssc3. We therefore speculate that in addition to this, there may be other amino acid residues that contribute to the conformational differences and a cumulative effect of multiple substitutions could be the cause for loss of chaperone function in Ssc3.

Analysis of the Functional Interaction with J-protein Co-chaperones and Nucleotide Exchange Factor of Mitochondrial Matrix—To demonstrate whether the conformational flexibility of the Ssc3 NBD affects its intrinsic activity in a full-length context, we analyzed the interaction with various co-chaperones. The nucleotide exchange factors are essential co-chaperones of the yeast mitochondrial matrix that accelerate the rate of exchange between ADP to ATP by several orders of magnitude in a typical folding reaction. Mge1 is the nucleotide exchange factor for yeast mitochondrial Hsp70s similar to *E. coli* GrpE. Ssc1 and Ssc3 as well as their respective NBDs interacted efficiently with Mge1 as analyzed by GST pulldown analysis ([supplemental Fig. S7, A–C](#)) and the interaction was found to be nucleotide sensitive ([supplemental Fig. S7, B and C](#)). To assess the kinetics of nucleotide release activity for Ssc3, we used the single turnover ATPase assay to monitor the hydrolysis of the prebound Ssc3-ATP complex in the presence of Mge1. Under single turnover conditions, both Ssc3 and Ssc1 showed similar basal ATPase activity with k_{cat} values of $0.056 \pm$

0.005 and $0.065 \pm 0.003 \text{ min}^{-1}$, respectively (data not shown). As indicated in Fig. 6A, a 2-fold excess of Mge1 showed robust nucleotide exchange activity, thus inhibiting the maximum ATP hydrolysis of Ssc3. Interestingly, however, under similar conditions, Ssc1 showed only 40% inhibition of ATP hydrolysis. The faster rate of nucleotide exchange kinetics by Mge1 for Ssc3 indicates a possible partial open conformation associated with NBD in the wild type protein. We further investigated the mechanisms of interaction between Ssc3 and J-protein co-chaperones that are responsible for the regulation of ATP hydrolysis by directly binding to NBD of Hsp70s. Yeast mitochondrial matrix contains the *E. coli* DnaJ homolog called Mdj1 that is required for folding reaction and Pam18, a J-protein co-chaperone essential for the translocation function. To assess the functional interaction of J-proteins with Ssc3 protein, we again utilized single turnover ATPase experiments. At a 1:1 molar ratio of Ssc3 to J-proteins, 6- and 4.5-fold stimulation was observed with Mdj1 and Pam18, respectively, for wild type protein (Fig. 6B, left and right panels). Interestingly, under similar conditions, Ssc1 showed very comparable levels of J-protein stimulation indicating that the J-protein interaction interface is relatively unaltered in the Ssc3 protein (Fig. 6B). Based on our results it is evident that the overall conformational plasticity associated with both domains of Ssc3 renders it unable to functionally complement Ssc1 in yeast mitochondria.

Impaired Inter-domain Allosteric Communication between SBD and NBD of Ssc3—Inter-domain allosteric communication plays a major role in modulating both ATP hydrolysis as well as the substrate binding activities of Hsp70s. In a typical Hsp70 chaperone cycle, the allosteric communication is bi-directional. Binding of ATP to the NBD triggers the release of substrates from SBD by converting it into a low affinity open conformation state. On the other hand, binding of substrate to the SBD triggers ATP hydrolysis in the NBD leading to a closed high affinity state. To identify whether Ssc3 possesses normal levels of allosteric inter-domain communication between SBD and NBD, we have tested different parameters including, substrate-mediated stimulation of ATPase activity, ATP-induced weakening of peptide binding, and ATP-induced changes in intrinsic tryptophan fluorescence.

As a first level of analysis for allosteric communication in Ssc3, we have tested the substrate-mediated stimulation of ATPase activity. Addition of 500-fold excess of the P5 peptide to the Ssc1·ATP complex led to 19-fold stimulation over the basal activity. This indicates that a robust peptide induced allosteric communication in Ssc1 (Fig. 7A). However, under similar conditions, only a meager 2-fold stimulating effect was observed for the Ssc3·ATP complex, indicating a significantly impaired peptide-mediated allosteric communication in Ssc3 (Fig. 7A). Even though Ssc3 and Ssc1 have a similar affinity for peptide in the ATP-bound form, the inability of the peptide to stimulate efficiently ATPase activity of Ssc3 suggests that, the inter-domain interface might be disrupted in Ssc3 resulting in an altered allosteric communication.

For further strengthening our observation, we analyzed the kinetics of peptide dissociation in the presence of ATP, a parameter used to study inter-domain coupling in Hsp70s (53). Addition of ATP to a preformed Hsp70·peptide complex results

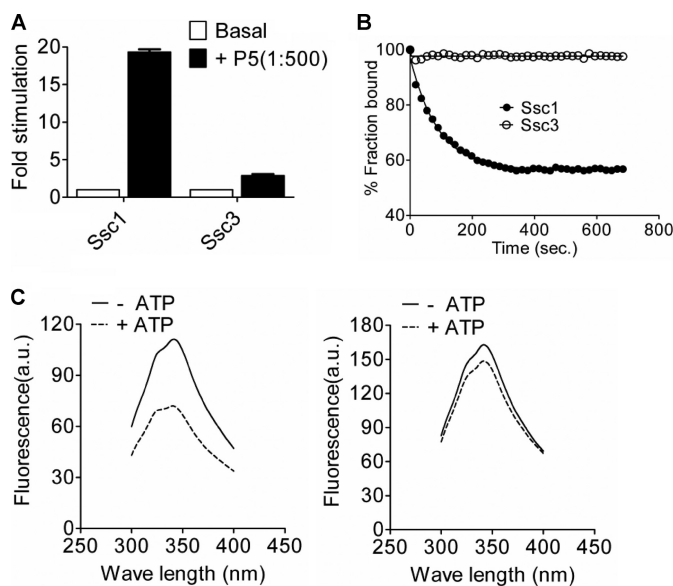


FIGURE 7. Study of ATP-induced conformational changes in Ssc1 and Ssc3. A, 1 μM radiolabeled ATP complexes of wild type Ssc1 and Ssc3 proteins were prepared and incubated with 500-fold excess of P5 substrate. ATP hydrolysis was monitored as a function of time at 25 °C. The percentage of ATP to ADP conversion at various time intervals was plotted and fitted into one-phase exponential association binding analysis to calculate the hydrolysis rate constant. Fold-stimulation was calculated by setting the intrinsic ATP hydrolysis rate as 1. B, the preformed Ssc1 (5 μM) or Ssc3·P5 complex (15 μM) was mixed with 1 mM ATP (final) and the loss of anisotropy was monitored kinetically at 12-s time intervals (right panel). C, 2 μM Ssc1 (left panel) or Ssc3 proteins (right panel) in buffer A in the absence (solid line) or presence (dashed line) of ATP was excited at 290 nm and emission spectra were recorded from 300 to 400 nm to measure the intrinsic tryptophan fluorescence.

in release of 50–60% of the prebound peptide due to conformational changes at the functional allosteric interface. Interestingly, when ATP was added to a prebound Ssc3·P5 complex, the bound peptide fluorescence level did not alter significantly as in comparison to Ssc1 (Fig. 7B). The inefficiency of releasing the bound peptide in the presence of ATP thus provides additional evidence for the altered allosteric regulation associated with Ssc3 protein.

To further examine the defect in inter-domain communication, we have utilized intrinsic tryptophan (Trp) fluorescence quenching analysis upon ATP binding. In DnaK, the decrease in intrinsic Trp fluorescence has been widely used for monitoring the allosteric conformational changes upon nucleotide binding (54, 55). The binding of ATP in DnaK leads to quenching of Trp residue (Trp-102) fluorescence and a blue shift of its emission maximum. Such spectroscopic changes require an efficient interaction between both domains (SBD and NBD) with a functional allosteric interface. Both Ssc3 and Ssc1 contain a similar “Trp” residue in NBD, which can be utilized for monitoring the conformational changes upon ATP binding. In the case of Ssc1, addition of ATP induces ~35% reduction of Trp fluorescence intensity (Fig. 7C, left panel). In contrast, Ssc3 showed only ~9% reduction in Trp fluorescence intensity (Fig. 7C, right panel). Taken together, collectively our observations clearly highlight a possible dysfunctional domain interface in Ssc3 leading to altered regulation of allosteric communication.

NBD Determines the Functional Specificity between Ssc3 and Ssc1 Paralogs—To define the minimal region of Ssc3 that is critical to functionally compensate for the *SSC1* null mutation,

Comparative Analysis of Divergent Yeast mtHsp70 Paralogs

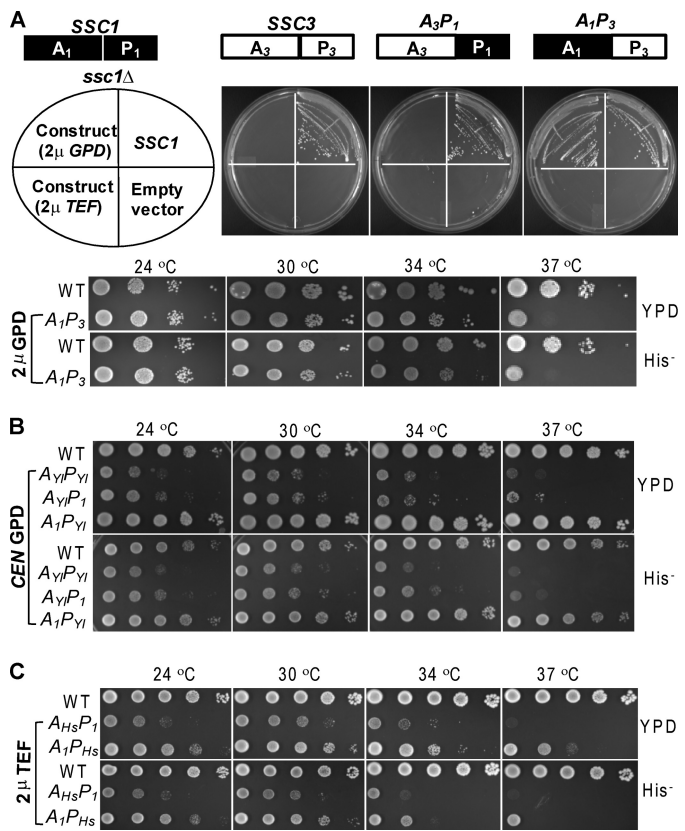


FIGURE 8. NBD of Ssc1 is critical for rescuing the lethality of the *ssc1Δ* strain. *A*, *ssc1Δ* cells expressing the wild type copy of the *SSC1* gene from a *URA* plasmid were transformed with either *SSC1* on a *CEN* plasmid or *SSC3* (*left panel*), *A₃P₁* (*middle panel*), or *A₁P₃* (*right panel*) from a 2μ *μPRS423* plasmid driven by either *TEF* or *GPD* promoters. 10-fold serial dilutions of an equivalent number of *ssc1Δ* cells expressing either Ssc1 from its own promoter (*WT*) or overexpressing *A₁P₃* from the 2μ *GPD* promoter were spotted on rich or selective medium and incubated at the indicated temperatures for 3 days. *B*, 10-fold serial dilutions of an equivalent number of *ssc1Δ* cells expressing either Ssc1 from its own promoter (*WT*) or overexpressing *A_yP_y*, *A_yP_y*, and *A_yP_y* from *CEN GPD* promoter, and *C*, overexpressing *A_{Hs}P_{Hs}* and *A_{Hs}P_{Hs}* from 2μ *TEF* promoter, were spotted on rich or selective medium and incubated at the indicated temperatures for 3 days.

we have generated chimeras between Ssc1 and Ssc3 proteins. The *A₁P₃* chimera was obtained by fusing the NBD of Ssc1 with SBD of Ssc3, whereas the *A₃P₁* chimera was generated by reverse swapping. To test *in vivo* complementation of *ssc1Δ* cells, both chimeras were overexpressed under *TEF* and *GPD* promoters using high copy 2μ plasmid. Interestingly, the *A₁P₃* chimera was able to rescue *ssc1Δ* cells in contrast to *A₃P₁* on 5-fluoroorotic acid counterselection medium (Fig. 8A, *middle* and *right panels*). However, the growth complementation of *ssc1Δ* cells was observed only when *A₁P₃* was overexpressed under the stronger *GPD* promoter. To check the phenotype of *ssc1Δ* cells complemented with *A₁P₃*, we have subjected them to drop test analysis using rich and minimal media at different temperature conditions. The *A₁P₃* chimera showed complete growth complementation at 30 °C, but was temperature sensitive at 37 °C as compared with wild type cells (Fig. 8A and *supplemental Table S5*). Our observations highlight that the NBD of Ssc1 plays a critical role in determining the functional specificity with the Ssc3 paralog.

To ascertain the critical role of NBD in defining the functional specificity across the species, we have generated chimeric

constructs between Ssc1 and its ortholog having similar function from a closely related species, *Yarrowia lipolytica*. Interestingly, full-length mtHsp70 of *Y. lipolytica* (*A_{Yl}P_{Yl}*) when expressed under the centromeric *GPD* promoter was able to complement *ssc1Δ* cells upon 5-fluoroorotic acid counterselection (*supplemental Fig. S8A, left panel*). This could be attributed to a high degree of sequence conservation and less functional divergence among phylogenetically clustered species. However, when subjected to drop test analysis, the above strain was found to be temperature sensitive at all temperatures tested (Fig. 8B and *supplemental Table S5*). To further dissect out the temperature-sensitive phenotype at the domain level, we made two different chimeric constructs by swapping each of the two domains of Ssc1 with that of mtHsp70 from *Y. lipolytica* (*A_{Yl}P_{Yl}*) (*supplemental Fig. S8A*). Importantly, the chimeric construct *A₁P_{Yl}* consisting of the NBD of Ssc1 fused to the SBD of its ortholog from *Y. lipolytica* was able to show complete growth complementation of *ssc1Δ* cells at all temperatures tested (Fig. 8B and *supplemental Table S5*). Notably, the reverse chimeric construct *A_{Yl}P₁*, consisting of NBD from *Y. lipolytica* and SBD of Ssc1, showed a temperature-sensitive phenotype similar to full-length *A_{Yl}P_{Yl}* (Fig. 8B and *supplemental Table S5*). Therefore our results provide direct experimental evidence to define the essential and critical roles of NBD of mtHsp70 in dictating the protein function.

To further validate this hypothesis across species, we chose to study the growth complementation of *ssc1Δ* cells using mtHsp70 from *Homo sapiens* (mortalin; *A_{Hs}P_{Hs}*), which is phylogenetically distant from *S. cerevisiae*. As anticipated, in *ssc1Δ* cells, mortalin (*A_{Hs}P_{Hs}*) was not able to substitute the function of Ssc1 (*supplemental Fig. S8B, left panel*). Interestingly, both chimeric constructs consisting of NBD from mortalin and SBD of Ssc1 (*A_{Hs}P₁*) and vice versa (*A₁P_{Hs}*) were able to rescue *ssc1Δ* cells when expressed under 2μ *TEF* promoter (*supplemental Fig. S8B, middle and right panels*). However, the chimera containing the NBD of Ssc1 (*A₁P_{Hs}*) showed better growth complementation at all temperatures tested in comparison to the other construct (*A_{Hs}P₁*) (Fig. 8C and *supplemental Table S5*). These results further emphasize the indispensable nature of NBD of a particular species in executing the specific essential *in vivo* functions of Hsp70.

DISCUSSION

Variations at the functional level are expected among genes that are retained in duplicate during evolution. In some instances, one copy may acquire a new function (neofunctionalization), whereas the other keeps the parental function. In the case of heat shock protein 70s, there are several duplicated paralogous genes that are stably retained in different cellular compartments as a subfunctionalized form or evolved to a newer function (56). The rate of evolutionary changes in the amino acid sequence within a defined protein segment or domain that leads to either sub- or neofunctionalization of duplicated *HSP70* paralogous genes are yet to be addressed. In the case of the *S. cerevisiae* mitochondrial matrix, there are 3 *HSP70* genes that have been retained for proper organelle biogenesis. Ssc1 is the constitutively and abundantly expressed mtHsp70 responsible for the majority of housekeeping func-

tions. On the other hand, the Ssq1 paralog retained in the sub-functionalized state is dedicated to robust generation of the Fe-S cluster in the mitochondrial matrix. However, the nature of subfunctionalization of the Ssc3 paralog in the mitochondrial matrix has been poorly understood. Although based on a high degree of sequence identity, it is hypothesized that Ssc1 and Ssc3 may share close overlapping housekeeping functions in the mitochondrial matrix (26). Strikingly, our results clearly disprove the hypothesis of overlapping functions between Ssc1 and Ssc3. Our *in vitro* biochemical observations and *in vivo* functional analysis demonstrate that Ssc3 cannot perform generic chaperone-specific functions due to its altered overall primary protein structure acquired following the gene duplication event. There are several key evidences presented here for validating our findings.

Foremost, our analysis reveals that Ssc3 possesses weaker affinity for client protein binding in the mitochondrial matrix. A significant reduction in affinity toward the pre-sequence derived peptides (P5) was observed in the ADP-bound state of Ssc3. Interestingly, however, in the ATP-bound state the affinity was found comparable with Ssc1. Although, the chaperone cycle is initiated in the ATP-bound state *in vivo*, the stabilization of the client-protein interaction in the ADP-bound state is critical to ensure proper folding (3, 4). Based on our biochemical data, we predict that even though Ssc3 possesses the ability to initiate the chaperone cycle in the ATP-bound state, the efficiency of folding of the newly imported or misfolded protein conformers will be significantly lower due to weaker affinity in the ADP-bound form. Furthermore, we speculate that the trapping ability of the translocating polypeptide would also be significantly altered due to poor affinity in the ADP-bound state thus limiting its ability to perform the import function as efficiently as Ssc1. Besides, SBD of Ssc3 failed to show any detectable physical interaction with the membrane tether, Tim44 protein. Based on our analysis, it is evident that Ssc3 is unlikely to replace Ssc1 as the core of “import motor” to perform robust translocation functions in *ssc1Δ* cells, due to impaired Tim44 and substrate interaction. Similarly, Ssc3 also displayed very poor affinity toward the native scaffold protein Isu1, on which a Fe-S cluster is built prior to transfer to a recipient apoprotein. Therefore, we predict that Ssc3 would fail to assemble a stable ISC-assembly complex thus limiting its role in the Fe-S cluster biogenesis in yeast mitochondria.

Our analysis reveals that the SBD of Ssc3 has acquired an “open conformation” due to amino acid sequence variation in the helical lid portion of the C terminus. The fluorescence anisotropy analysis demonstrates that Ssc3 possesses a 80-fold faster substrate release rate in the ADP-bound state in comparison to Ssc1 that resembles closely the ATP-bound conformation of generic Hsp70s. Furthermore, the affinity of Ssc3 in the ADP- or ATP-bound forms was found to be comparable further supporting the possibility of an open conformational state. Therefore, we hypothesize that the helical lid region of Ssc3 does not tightly associate over the peptide binding cleft thus enhancing the dissociation rate of the substrate in the ADP-bound state. Additionally, these findings are further supported by helical lid deletion mutants (Ssc3₅₅₈ and Ssc3₅₂₈) that showed affinity similar to wild type Ssc3 in the ADP-bound

state. To uncover the molecular reasons for such an open conformation of SBD of Ssc3, we have utilized chimeric proteins of Ssc3 and Ssc1 by systematically interchanging different helices from the helical lid region. Most interestingly, the Ssc3 chimeric protein containing the D-helix of Ssc1 showed significant improvement in the ability to bind substrates in the ADP-bound state in comparison to wild type Ssc3. Retrospectively, the chimeric Ssc1 protein containing the D-helix of Ssc3 results in a significant reduction in substrate binding and its affinity was found to be comparable with the atypical Ssc3 paralog. This finding conclusively proves that the primary sequence spanning the D-helix of mtHsp70s determines the affinity toward mitochondrial client proteins. Based on our observations we hypothesize that the D-helix perhaps regulates positioning of the lid region over the SBD-cleft thereby controlling the substrate binding in ADP- and ATP-bound states in mtHsp70 paralogs.

Second, the conformational stability of Ssc3 is remarkably low and strongly prone to aggregation and thus failed to complement Hsp70-specific functions *in vivo*. Most of the generic Hsp70s exhibit at least two prominent thermal transitions for each of their respective domains. As reported earlier for DnaK, the T_m of NBD was centered around 41 °C, whereas SBD was closer to 70 °C (28, 49). Strikingly, our observation shows that Ssc3 possesses a single T_m centered around 30 °C that is remarkably low in comparison to generic Hsp70s. The overall reduced stability of the Ssc3 protein is attributable to the relative alterations in the conformation of both domains as well as positioning of the linker region. The limited proteolysis data clearly highlights that the rate of trypsin cleavage of Ssc3 was significantly faster than Ssc1. Moreover, the apparent lack of accumulation of a stable fragment in Ssc3 implies gross conformational differences between Ssc3 and Ssc1. Besides, the individual purified NBD and SBD also showed a significantly faster rate of trypsin cleavage as in comparison to the respective domains of Ssc1. These findings suggest that conformational changes have occurred across both domains upon sequence diversification following gene duplication events.

At non-permissive temperature conditions, Ssc3 exhibits inherent tendency for aggregation in mitochondria due to the reduced conformational stability of the protein. A similar aggregation pattern was observed even when Ssc3 was co-expressed with Zim17 in *E. coli* cells at 37 °C. Importantly, the reduced thermal stability of Ssc3 under *in vivo* conditions was found comparable with *in vitro* analysis wherein the purified protein showed a strong tendency to aggregate at higher temperatures. However, based on our analysis we rule out the possibility that Ssc3 aggregation is due to its inability to interact with Zim17 in mitochondria as well as in *E. coli* cells. Rather, we speculate that Zim17 failed to rescue a high degree of conformational plasticity associated with Ssc3 at higher temperatures as compared with the other stable Hsp70s such as Ssc1. Furthermore, our results demonstrate that the aggregation property of the wild type protein is primarily associated with the NBD. These findings are consistent with recent reports dealing with the coexpression analysis of Ssc3 in *E. coli* (39). To identify the critical residues that contribute to the aggregation propensity of Ssc3, we have generated a series of mutants in

Comparative Analysis of Divergent Yeast mtHsp70 Paralogs

Ssc1 using the diverged sequence from Ssc3. Most notably, the $\text{Ssc1}_{\text{G160A}, \text{P162S}}$ mutant showed enhanced aggregation, whereas on the other hand, reverse mutation in Ssc3 ($\text{Ssc3}_{\text{A157G}, \text{S159P}}$) showed reduced aggregation and a corresponding increase in solubility. In the DnaK structure, both residues at their respective positions were exposed at the interface between SBD and NBD. Therefore, we speculate that these residues might play a crucial role in positioning of inter-domain linker region, hence regulating the aggregation propensity as well as allosteric communication between SBD and NBD. However, we do not rule out the possibility that the conformational differences between the two proteins could be due to a cumulative effect of multiple amino acid substitutions, as the double mutant showed only $\sim 25\text{--}30\%$ reduction in solubility, which is insufficient to account for the high aggregation propensity of Ssc3.

Third, Ssc3 possesses a dysfunctional inter-domain interface thus rendering it unable to perform generic Hsp70-specific functions in yeast mitochondria. A dynamic equilibrium between low- and high-affinity states of Hsp70 is critical for the *in vivo* chaperone cycle (1–3). There are several allosteric regulators such as nucleotides, co-chaperones, and client proteins that modulate the chaperone cycle by altering the inter-domain interface through a series of distinct conformational changes across NBD and SBD. Surprisingly, Ssc3 failed to show the effect of such allosteric regulators as compared with Ssc1. The experimental measurements involving ATP-dependent release of substrate, intrinsic fluorescence quenching upon ATP binding, and substrate-mediated ATPase stimulation explicitly demonstrated that Ssc3 possesses a significant bidirectional allosteric communication defect thus reducing its overall efficiency of chaperone function.

Fourth, the rate of nucleotide exchange activity of Ssc3 in the presence of Mge1 was dramatically faster than generic Hsp70s. The nucleotide exchange factors such as bacterial GrpE and yeast Mge1 are critical components of the chaperone machinery. The nucleotide exchange factors accelerate the exchange of nucleotides (ADP to ATP) thus regulating the equilibrium between high and low affinity states of Hsp70s (1, 7). Interestingly, Ssc3 showed a very high rate of nucleotide exchange with Mge1 as compared with Ssc1. However, the levels of Mge1 interaction with Ssc3 and Ssc1 were found to be comparable. Therefore, we propose that the faster rate of nucleotide exchange activity of Ssc3 is possibly due to the partial open conformation of the NBD. In addition, we speculate that the fast nucleotide exchange would be equally deleterious to cells because it is likely to alter the dynamic equilibrium of different nucleotide states of Hsp70s thus disfavoring a functional overlap with Ssc1.

Finally, our results provide the first direct experimental evidence to demonstrate that the NBD region of Hsp70 is critical for functional overlap between paralogs and orthologs. The NBD of generic Hsp70s is highly regulated through many co-chaperone interactions that are essential for *in vivo* functions. In the yeast mitochondrial matrix, mtHsp70 (Ssc1) consists of a distinct NBD region co-evolved together with other co-chaperone machinery such as J-proteins, nucleotide exchange factors, and Hep1 for optimized cellular functions. Hence, NBD of Ssc1 functionally cannot be completely replaced by paralogs such as

Ssc3 or orthologs from other species having similar functions. In agreement with this, all chimeras generated that lack the NBD of Ssc1 either failed to rescue $\text{ssc1}\Delta$ cells or showed poor growth complementation at all conditions tested, suggesting its critical requirement for *in vivo* functions. In retrospect, chimeras consisting of the NBD of Ssc1 and SBDs of paralogs and orthologs having similar functions were able to show better growth complementation of $\text{ssc1}\Delta$ cells at all temperatures tested. The extent of growth complementation by chimeric proteins is varied due to differences in the relative affinity for mitochondrial client protein binding by the paralogs and orthologs of SBD. For example, the A_1P_3 chimeric protein consisting of the SBD of Ssc3 was able to rescue the function of Ssc1 only upon high expression under the *GPD* promoter using the 2μ plasmid due to weak affinity toward client proteins. On the other hand, A_1P_{Y1} and A_1P_{Hs} chimeric proteins consisting of the SBD of the mtHsp70s from *Y. lipolytica* and *H. sapiens*, respectively, were able to rescue the function of Ssc1 at lower levels of expression, due to relatively better client protein binding affinity as in comparison to Ssc3 (23, 27). Therefore, we propose that the SBD of Ssc1 is selectively required for optimum growth under non-permissive conditions. In summary, taken together with our biochemical data, it is evident that the inability of Ssc3 to functionally complement the phenotype of Ssc1 is primarily attributable to the conformational plasticity associated with its NBD. The Ssc3 paralog is retained only in a smaller subset of closely related fungi such as *S. cerevisiae*, *Saccharomyces bayanus*, and *Candida glabrata* species (23). However, the genomes of other fungal species such as *Y. lipolytica*, *Neurospora crassa*, and *Schizosaccharomyces pombe* do not harbor the *SSC3* copy similar to higher eukaryotes (23). Based on our analysis, we envisioned that the evolutionary loss of the *SSC3* gene is likely due to a weak chaperone function as well as asymmetric evolution under lack of selective pressure. Furthermore, our findings establish that the NBD is the minimal region of generic Hsp70s required for functional overlap between paralogs and orthologs. Therefore, we hypothesize that sequence divergence following gene duplication in the NBD region of Hsp70s defines the functional specificity of Hsp70 within and across the kingdoms. Our analysis on Ssc3 and Ssc1 paralogs will provide a basic platform for future investigation to uncover the functional specificity among Hsp70s of different cellular compartments.

Acknowledgments—We are grateful to Dr. Elizabeth A. Craig, Dr. Brenda Schilke, and William Walter for providing the yeast strain and antibodies against Hsp60, Tim23, and Mge1. We also thank Arvind Vittal Goswami for helpful discussions and insightful comments on the manuscript.

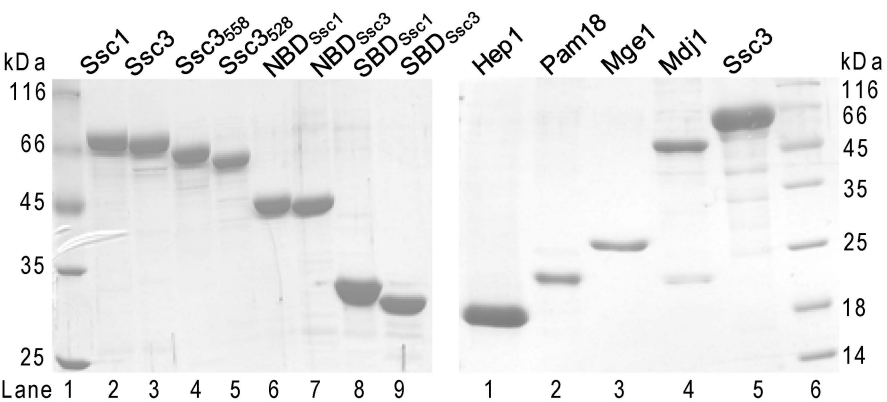
REFERENCES

1. Mayer, M. P., and Bukau, B. (2005) *Cell. Mol. Life Sci.* **62**, 670–684
2. Hartl, F. U., and Hayer-Hartl, M. (2002) *Science* **295**, 1852–1858
3. Bukau, B., Weissman, J., and Horwich, A. (2006) *Cell* **125**, 443–451
4. Hartl, F. U. (1996) *Nature* **381**, 571–579
5. Brocchieri, L., Conway de Macario, E., and Macario, A. J. (2008) *BMC Evol. Biol.* **8**, 19
6. Bettencourt, B. R., and Feder, M. E. (2001) *Mol. Biol. Evol.* **18**, 1272–1282

Comparative Analysis of Divergent Yeast mtHsp70 Paralogs

7. Craig, E. A., and Marszalek, J. (2002) *Cell. Mol. Life Sci.* **59**, 1658–1665
8. Craig, E. A., Kramer, J., Shilling, J., Werner-Washburne, M., Holmes, S., Kosic-Smithers, J., and Nicolet, C. M. (1989) *Mol. Cell. Biol.* **9**, 3000–3008
9. Kang, P. J., Ostermann, J., Shilling, J., Neupert, W., Craig, E. A., and Pfanner, N. (1990) *Nature* **348**, 137–143
10. Chacinska, A., Koehler, C. M., Milenkovic, D., Lithgow, T., and Pfanner, N. (2009) *Cell* **138**, 628–644
11. Neupert, W., and Herrmann, J. M. (2007) *Annu. Rev. Biochem.* **76**, 723–749
12. de Marcos-Lousa, C., Sideris, D. P., and Tokatlidis, K. (2006) *Trends Biochem. Sci.* **31**, 259–267
13. Schmidt, O., Pfanner, N., and Meisinger, C. (2010) *Nat. Rev. Mol. Cell Biol.* **11**, 655–667
14. D'Silva, P. D., Schilke, B., Walter, W., Andrew, A., and Craig, E. A. (2003) *Proc. Natl. Acad. Sci. U.S.A.* **100**, 13839–13844
15. Truscott, K. N., Voos, W., Frazier, A. E., Lind, M., Li, Y., Geissler, A., Dudek, J., Müller, H., Sickmann, A., Meyer, H. E., Meisinger, C., Guiard, B., Rehling, P., and Pfanner, N. (2003) *J. Cell Biol.* **163**, 707–713
16. Mokranjac, D., Sichting, M., Neupert, W., and Hell, K. (2003) *EMBO J.* **22**, 4945–4956
17. D'Silva, P. R., Schilke, B., Walter, W., and Craig, E. A. (2005) *Proc. Natl. Acad. Sci. U.S.A.* **102**, 12419–12424
18. Kozany, C., Mokranjac, D., Sichting, M., Neupert, W., and Hell, K. (2004) *Nat. Struct. Mol. Biol.* **11**, 234–241
19. Frazier, A. E., Dudek, J., Guiard, B., Voos, W., Li, Y., Lind, M., Meisinger, C., Geissler, A., Sickmann, A., Meyer, H. E., Bilanchone, V., Cumsky, M. G., Truscott, K. N., Pfanner, N., and Rehling, P. (2004) *Nat. Struct. Mol. Biol.* **11**, 226–233
20. Rowley, N., Prip-Buus, C., Westermann, B., Brown, C., Schwarz, E., Barrell, B., and Neupert, W. (1994) *Cell* **77**, 249–259
21. Laloraya, S., Gambill, B. D., and Craig, E. A. (1994) *Proc. Natl. Acad. Sci. U.S.A.* **91**, 6481–6485
22. Schilke, B., Forster, J., Davis, J., James, P., Walter, W., Laloraya, S., Johnson, J., Miao, B., and Craig, E. (1996) *J. Cell Biol.* **134**, 603–613
23. Schilke, B., Williams, B., Knieszner, H., Pukszta, S., D'Silva, P., Craig, E. A., and Marszalek, J. (2006) *Curr. Biol.* **16**, 1660–1665
24. Strub, A., Röttgers, K., and Voos, W. (2002) *EMBO J.* **21**, 2626–2635
25. Sakasegawa, Y., Hachiya, N. S., Tsukita, S., and Kaneko, K. (2003) *Biochem. Biophys. Res. Commun.* **309**, 217–221
26. Baumann, F., Milisav, I., Neupert, W., and Herrmann, J. M. (2000) *FEBS Lett.* **487**, 307–312
27. Goswami, A. V., Chittoor, B., and D'Silva, P. (2010) *J. Biol. Chem.* **285**, 19472–19482
28. Montgomery, D. L., Morimoto, R. I., and Giersch, L. M. (1999) *J. Mol. Biol.* **286**, 915–932
29. Horst, M., Oppliger, W., Rospert, S., Schönfeld, H. J., Schatz, G., and Azem, A. (1997) *EMBO J.* **16**, 1842–1849
30. Sichting, M., Mokranjac, D., Azem, A., Neupert, W., and Hell, K. (2005) *EMBO J.* **24**, 1046–1056
31. Sinha, D., Joshi, N., Chittoor, B., Samji, P., and D'Silva, P. (2010) *Hum. Mol. Genet.* **19**, 1248–1262
32. Slutsky-Leiderman, O., Marom, M., Iosefson, O., Levy, R., Maoz, S., and Azem, A. (2007) *J. Biol. Chem.* **282**, 33935–33942
33. Mayer, M. P., Schröder, H., Rüdiger, S., Paal, K., Laufen, T., and Bukau, B. (2000) *Nat. Struct. Biol.* **7**, 586–593
34. Liu, Q., Krzewska, J., Liberek, K., and Craig, E. A. (2001) *J. Biol. Chem.* **276**, 6112–6118
35. Buchberger, A., Theyssen, H., Schröder, H., McCarty, J. S., Virgallita, G., Milkereit, P., Reinstein, J., and Bukau, B. (1995) *J. Biol. Chem.* **270**, 16903–16910
36. Miao, B., Davis, J. E., and Craig, E. A. (1997) *J. Mol. Biol.* **265**, 541–552
37. Ram, A. F., and Klis, F. M. (2006) *Nat. Protoc.* **1**, 2253–2256
38. Davis, J. E., Voisine, C., and Craig, E. A. (1999) *Proc. Natl. Acad. Sci. U.S.A.* **96**, 9269–9276
39. Blamowska, M., Sichting, M., Mapa, K., Mokranjac, D., Neupert, W., and Hell, K. (2010) *J. Biol. Chem.* **285**, 4423–4431
40. Lussier, M., White, A. M., Sheraton, J., di Paolo, T., Treadwell, J., Southard, S. B., Horenstein, C. I., Chen-Weiner, J., Ram, A. F., Kapteyn, J. C., Roemer, T. W., Vo, D. H., Bondoc, D. C., Hall, J., Zhong, W. W., Sdicu, A. M., Davies, J., Klis, F. M., Robbins, P. W., and Bussey, H. (1997) *Genetics* **147**, 435–450
41. Voisine, C., Craig, E. A., Zufall, N., von Ahsen, O., Pfanner, N., and Voos, W. (1999) *Cell* **97**, 565–574
42. Buczynski, G., Slepakov, S. V., Sehorn, M. G., and Witt, S. N. (2001) *J. Biol. Chem.* **276**, 27231–27236
43. Slepakov, S. V., Patchen, B., Peterson, K. M., and Witt, S. N. (2003) *Biochemistry* **42**, 5867–5876
44. D'Silva, P., Liu, Q., Walter, W., and Craig, E. A. (2004) *Nat. Struct. Mol. Biol.* **11**, 1084–1091
45. Lill, R., and Mühlhoff, U. (2008) *Annu. Rev. Biochem.* **77**, 669–700
46. Knieszner, H., Schilke, B., Dutkiewicz, R., D'Silva, P., Cheng, S., Ohlson, M., Craig, E. A., and Marszalek, J. (2005) *J. Biol. Chem.* **280**, 28966–28972
47. Sehorn, M. G., Slepakov, S. V., and Witt, S. N. (2002) *Biochemistry* **41**, 8499–8507
48. Fernández-Sáiz, V., Moro, F., Arizmendi, J. M., Acebrón, S. P., and Muga, A. (2006) *J. Biol. Chem.* **281**, 7479–7488
49. Swain, J. F., Dinler, G., Sivendran, R., Montgomery, D. L., Stotz, M., and Giersch, L. M. (2007) *Mol. Cell* **26**, 27–39
50. Momose, T., Ohshima, C., Maeda, M., and Endo, T. (2007) *EMBO Rep.* **8**, 664–670
51. Zhai, P., Stanworth, C., Liu, S., and Silberg, J. J. (2008) *J. Biol. Chem.* **283**, 26098–26106
52. Bertelsen, E. B., Chang, L., Gestwicki, J. E., and Zuiderweg, E. R. (2009) *Proc. Natl. Acad. Sci. U.S.A.* **106**, 8471–8476
53. Slepakov, S. V., and Witt, S. N. (2002) *Biochemistry* **41**, 12224–12235
54. Vogel, M., Mayer, M. P., and Bukau, B. (2006) *J. Biol. Chem.* **281**, 38705–38711
55. Vogel, M., Bukau, B., and Mayer, M. P. (2006) *Mol. Cell* **21**, 359–367
56. Rastogi, S., and Liberles, D. A. (2005) *BMC Evol. Biol.* **5**, 28

Supplemental Fig. S1



Supplemental Fig. S1:

SDS-PAGE analysis of purified Ssc1, Ssc3 and their variants. *A*, 5 µg of different proteins are separated on 12.5% SDS-PAGE: molecular weight marker (*lane 1*), Ssc1 (*lane 2*), Ssc3 (*lane 3*), Ssc₃₅₅₈ (*lane 4*), Ssc₃₅₂₈ (*lane 5*), NBD_{Ssc1} (*lane 6*), NBD_{Ssc3} (*lane 7*), SBD_{Ssc1} (*lane 8*), SBD_{Ssc3} (*lane 9*). *B*, SDS-PAGE analysis of recombinantly expressed and purified Hep1 (*lane 1*), Pam18 (*lane 2*), Mge1 (*lane 3*), Mdj1 (*lane 4*), Ssc3 (*lane 5*) and molecular weight marker (*lane 6*).

Supplemental Fig. S2

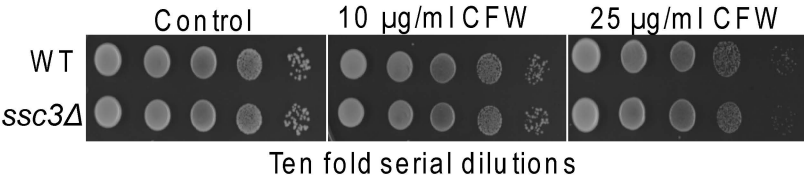
A

| | | | | | |
|----------|--|------------|-----------|------------|--|
| Ssc1 | MIAAKNILNRSSLSSSERIATRLQSTKVQGSVIGIDLGTTNSAVAIMEGKVPKIIENAEQ | 60 | | | |
| Ssc3 | MIPSWKAFKAHNI---LRILTRFQSTKIPDAVIGIDLGTTNSAVAIMEGKVPRIIENAEQ | 57 | | | |
| Ssc1 | SRTTPSVAFTKEGERLVGIPAKRQAVNPENTLFATKRLIGRRFEDAEVQRDIKQVPYK | 120 | | | |
| Ssc3 | SRTTPSVAFTKDGERLVEPAKRQSVINSENTLFATKRLIGRRFEDAEVQRDINQVPFK | 117 | | | |
| Ssc1 | IVKHSNGDAWVEARGQTYSAPAQIGGFVLNKMKTAEAYLGKPVKNAVVTVPAYFNDSQRQ | 180 | | | |
| Ssc3 | IVKHSNGDAWVEARNRTYSAPAQIGGFIILNKMKTAEAYLAQSVKNAVVTVPAYFNDAQRQ | 177 | | | |
| Ssc1 | ATKDAGQIVGLNVLRVVNEPTAAALAYGLEKSDSKVAVFDLGGGTFDISILDIDNGVFE | 240 | | | |
| Ssc3 | ATKDAGQIIGLNVLRVVNEPTAAALAYGLDKSEPKVIAVFDLGGGTFDISILDIDNGIFE | 237 | | | |
| Ssc1 | VKSTNGDTHLGGEDFDIYLLREIVSRFKTETGIDLENDRMAIQRIEAAEKAKIELSSTV | 300 | | | |
| Ssc3 | VKSTNGDTHLGGEDFDIYLLQEIIISHKETGIDLSNDRMAVQRRIEAAEKAKIELSSTL | 297 | | | |
| Ssc1 | STEINLPFITADASGPKHINMKFSRAQFETLTAPIVKRTVDPVKKALKDAGLSTS DISEV | 360 | | | |
| Ssc3 | STEINLPFITADAAGPKHIRMPFSRVQLENITAPLIDRTVDPVKKALKDARITASDSDV | 357 | | | |
| Ssc1 | LLVGGMSRMPKVETVKSLFGKDPSKAVNPDEAVAIGAAVQGAVLSGEVDVLLDV | 417 | | | |
| Ssc3 | LLVGGMSRMPKVA DTVK KLFKGKDASKAVNPDEAVALGAAIQAAVLSGEVDVLLDV | 414 | | | |
| B | | | | | |
| | $\beta 1$ | $\beta 2$ | $\beta 3$ | $\beta 4$ | |
| Ssc1 | DVLLLDVTPLSLGIETLGGVFTRLIPRNTTIPKKSQIFSTAAAGQTSVEIRVFQGEREL | 60 | | | |
| Ssc3 | DVLLLDVTPLSLGIETLGGVFTKLIPRNSTIPNKKSQIFSTAAAGQTSVEVKVFQGEREL | 60 | | | |
| | $\beta 5$ | $\beta 6$ | $\beta 7$ | $\beta 8$ | |
| Ssc1 | VRDNKLIGNFTLAGIPPAPKGVPQIEVTFDIDADGIINVSARDKATNKKDSSITVAGSSGL | 120 | | | |
| Ssc3 | VKDNKLIGNFTLAGIPPAPKGTPQIEVTFDIDANGIINVSAKDLASHKDSSITVAGASGL | 120 | | | |
| | αA | αB | | αC | |
| Ssc1 | SENEIEQMVNDAEKFKSQDEARKQAIETANKADQLANDTENSILKEFEGKVDKAEEAQKVRD | 180 | | | |
| Ssc3 | SDTEIDRMVNNEARYKNQDRARRNAIETANKADQLANDTENSIKEFEGKLDKTDSQLKD | 180 | | | |
| | αD | αE | | | |
| Ssc1 | QITSILKELVARVQGGEVNAAEELKTKTEELQTS SSMKLFEQLYKNDNNNNNNNGNNAESG | 240 | | | |
| Ssc3 | QISSILRELVRSRSQAGDEVNDDVGTKIDNLRTSSMKLFEQLYKN-SDNPETKNGR----- | 234 | | | |
| Ssc1 | ETKQ 244 | | | | |
| Ssc3 | ENK- 237 | | | | |

Supplemental Fig. S2:

Sequence comparison of Ssc1 and Ssc3. *A*, Sequence alignment of nucleotide-binding domain (NBD); and *B*, substrate-binding domain (SBD) of Ssc1 and Ssc3 using ClustalW2 tool. Identical amino acids are shaded by gray boxes. Secondary structure elements including β strands ($\beta 1-\beta 8$) and α helices ($\alpha A-\alpha E$) are indicated by modelling the structure of Ssc1 using Pymol software and structure of DnaK as a template (2KHO1).

Supplemental Fig. S3

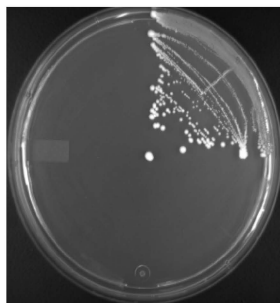
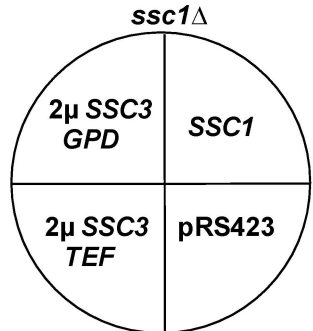


Supplemental Fig. S3:

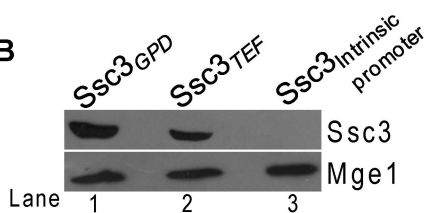
Calcofluor white (CFW) hypersensitivity test of *ssc3Δ* strain. CFW hypersensitivity of *ssc3Δ* strain was checked by drop test on YPD plates containing 10 μ g/ml (*middle panel*) and 25 μ g/ml (*right panel*) of CFW solution. Parent strain BY4741 *MATa* (*his3Δ1 leu2Δ met15Δ ura3Δ*) was used as a control.

Supplemental Fig. S4

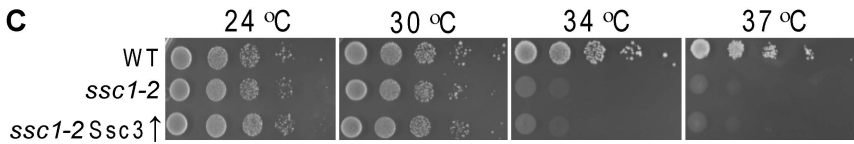
A



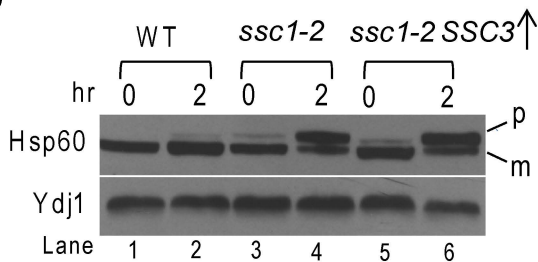
B



C



D

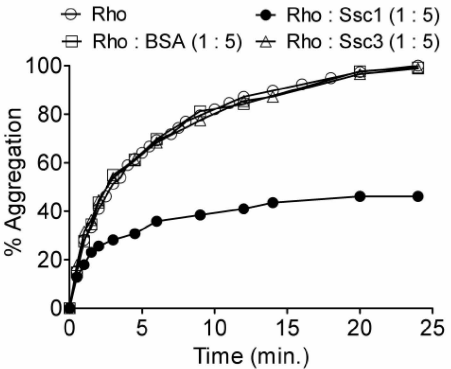


Supplemental Fig. S4:

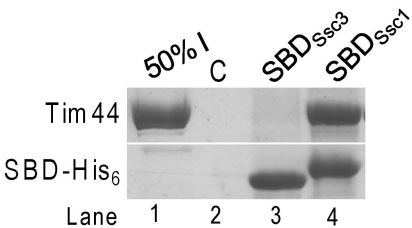
Growth complementation analysis of *ssc1Δ* cells upon Ssc3 overexpression. *A*, Haploid *ssc1Δ* strain expressing wild type copy of *SSC1* gene from a *URA* plasmid was transformed with either *SSC1* on a *CEN* plasmid or *SSC3* from a high copy pRS423 plasmid driven by *TEF* or *GPD* promoter. The cells were streaked on media containing 5-fluoroorotic acid and grown at 30 °C for 3 days. The empty pRS423 plasmid was used as a vector control. *B*, Total lysates prepared from cells overexpressing HA-tagged Ssc3 under different promoters as indicated were resolved by SDS-PAGE, electroblotted, and immunodecorated with anti-HA antibodies. Mge1 was used as a loading control. *C*, 10-fold serial dilutions of an equivalent number of *ssc1Δ* cells expressing either wt Ssc1 from its own promoter (WT), or *ssc1-2*, or *ssc1-2* overexpressing wild type Ssc3 from *GPD* promoter (*ssc1-2 Ssc3↑*) were spotted on selective medium and incubated at indicated temperatures for 3 days. *D*, Wild type (WT), *ssc1-2* and *ssc1-2 Ssc3↑* yeast strains were grown at permissive temperatures in minimal media to early log phase. The culture was shifted to 37 °C for 2 h to induce the temperature sensitive phenotype. Subsequently, the whole cell lysates were resolved by SDS-PAGE followed by immunoblotting using Hsp60-specific antibodies; (p), precursor form of Hsp60; (m), mature form of Hsp60.

Supplemental Fig. S5

A



B

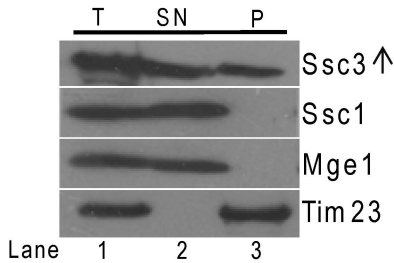


Supplemental Fig. S5:

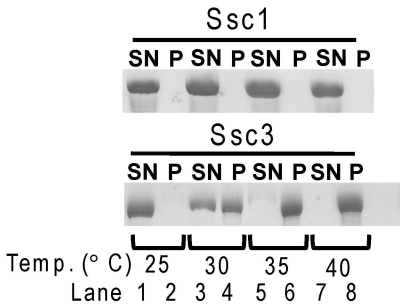
In vitro analysis of chaperone like activity of Ssc3 by rhodanese aggregation assay and Tim44 interaction. A, Bovine rhodanese was first denatured in 6 M guanidine hydrochloride and subsequently diluted into the reaction mixture and absorbance changes at 320 nm were used to monitor aggregation at different time intervals at 25 °C. Aggregation of denatured rhodanese (0.46 µm) in the presence of either 2.3 µM of Ssc1 or Ssc3 was monitored for 25 min by measuring the changes in turbidity. Percent aggregation values were plotted against time. Under similar conditions, 0.46 µm denatured rhodanese alone was used as an internal control (absence of chaperones) and in the presence of 4.6 µm bovine serum albumin (BSA) as a negative control. B, 4 µM of His-tagged SBDs of Ssc1 and Ssc3 were preincubated with 1 µM of non-tagged Tim44 in buffer F (20 mM HEPES pH 7.5, 100 mM KCl, 0.2 % Triton and 10 mM imidazole) for binding at 20 °C for 15 min. The reactions were then incubated with 10 µl of Ni-NTA resin (bed volume) for 30 minutes. The resin was washed 3 times with buffer F and bound proteins were analysed by SDS-PAGE followed by Coomassie dye staining. 50% of the input was used as loading control and Ni-NTA resin alone (absence of SBDs of Ssc1/Ssc3) used as negative control (C).

Supplemental Fig. S6

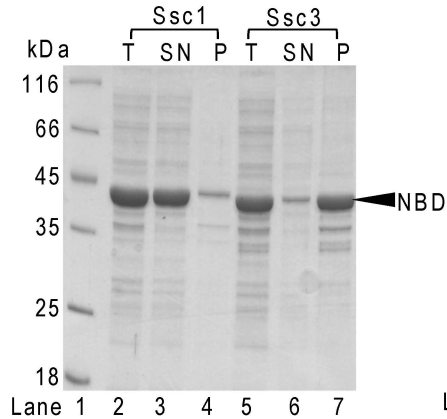
A



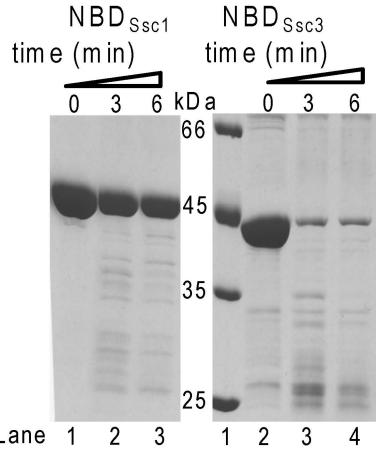
B



C



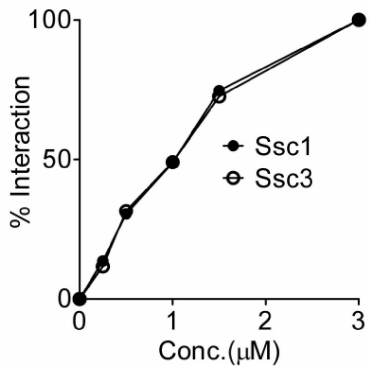
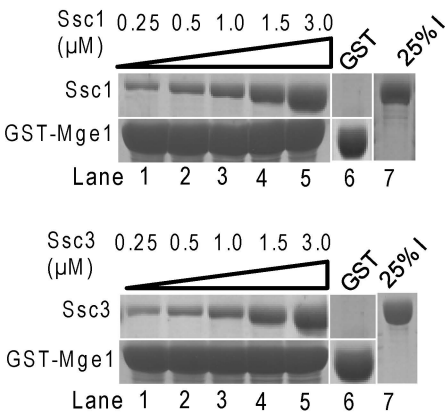
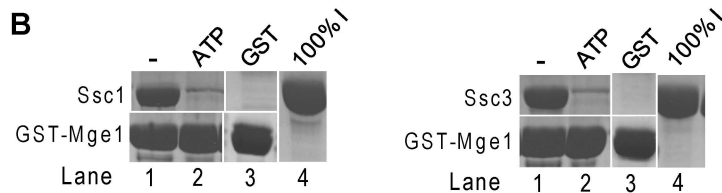
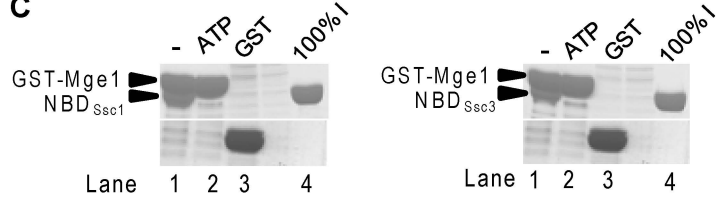
D



Supplemental Fig. S6:

Analysis of alteration in stability and solubility of Ssc3 upon overexpression. *A*, Mitochondria from Ssc3 overexpressing yeast strains (under Ssc1 promoter) were isolated and subjected to fractionation using sonication by hypotonic swelling method. The sonicated mitochondrial samples were subjected to ultracentrifugation. The equivalent amounts of supernatant (S) and pellet (P), and unfractionated extract (T) were analyzed by SDS-PAGE and immunoblotted with yeast specific antibodies as indicated. *B*, Thermal stability of Ssc1 (*top panel*) and Ssc3 (*bottom panel*) were analyzed by incubating the proteins at indicated temperatures for 30 min in buffer A containing 5% glycerol. The samples were separated into a supernatant (SN) and pellet (P) fraction by centrifugation and analyzed by SDS-PAGE followed by Coomassie dye staining. *C*, The NBDs of Ssc1 and Ssc3 along with the linker region were coexpressed with Hep1 in *E. coli* cells. The cells were lysed as described above and analyzed for its solubility by SDS-PAGE. *D*, 5 µg of NBDs of Ssc1 (*left panel*) and Ssc3 (*right panel*) were subjected to partial tryptic digestion as a function of time as described in Fig. 2. The samples were analyzed on SDS-PAGE and subjected to Coomassie dye staining.

Supplemental Fig. S7

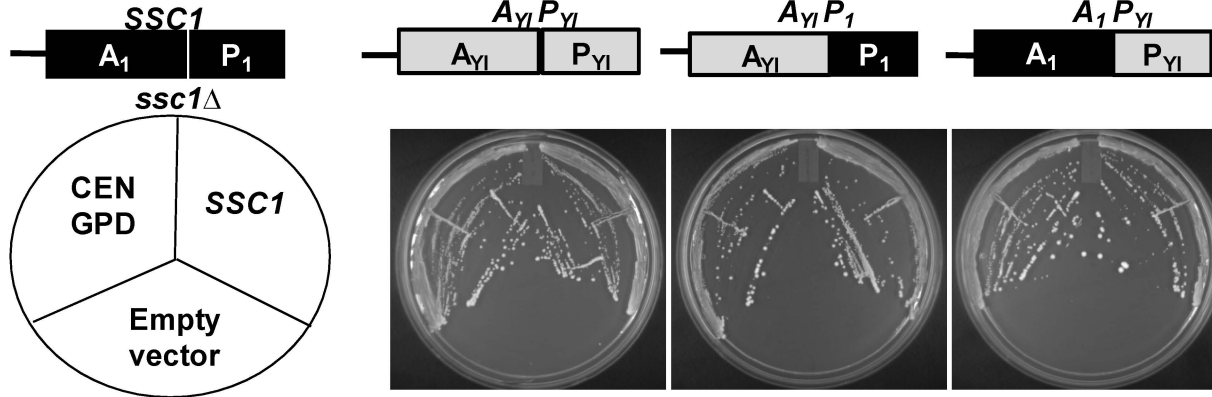
A**B****C**

Supplemental Fig. S7:

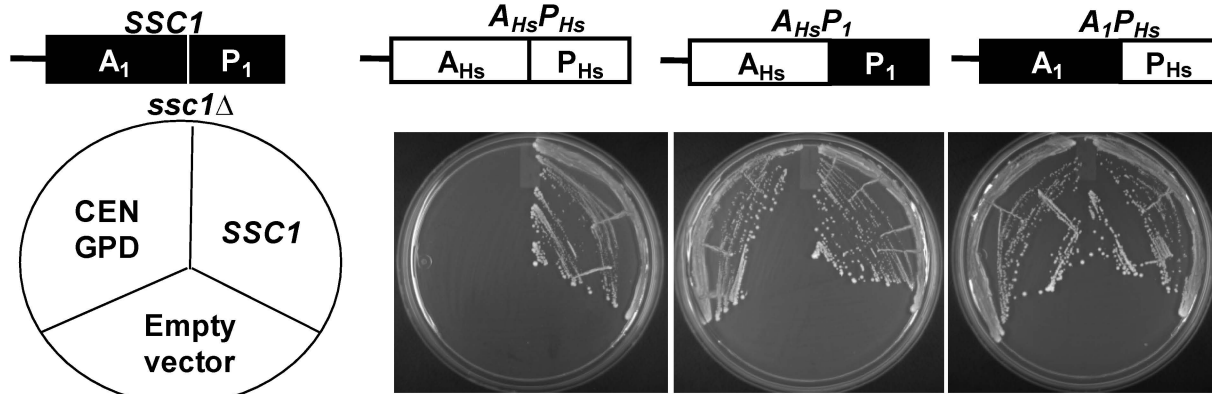
Nucleotide-dependent Mge1 interaction analysis of Ssc1, Ssc3 and their respective NBDs. *A*, Immobilized GST-Mge1 (1.5 μ M) was incubated with increasing concentrations of full-length Ssc1 (*left top panel*) and Ssc3 (*left bottom panel*) as indicated in the absence of nucleotides. The bound proteins were analyzed by SDS-PAGE followed by Coomassie dye staining. GST alone was used as a negative control and 25% input (offered to the beads) was used as a loading control. The data was quantified by densitometric analysis using ImageQuant software (*right panel*). *B*, Immobilized GST-Mge1 (1.5 μ M) was incubated with 2.5 μ M of full-length Ssc1 (*left panel*) and Ssc3 (*right panel*) in the presence or absence of 250 μ M of ATP. *C*, 1.5 μ M of immobilized GST-Mge1 was incubated with 2.0 μ M of NBD_{Ssc1} (*left panel*) and NBD_{Ssc3} (*right panel*) in the presence or absence of 250 μ M of ATP. The bound proteins were analyzed by SDS-PAGE followed by Coomassie dye staining. GST alone was used as a negative control and 100% input was used as a loading control.

Supplemental Fig. S8

A



B



Supplemental Fig. S8:

5-FOA counterselection of *ssc1Δ* cells complemented with various mtHsp70 constructs. The *ssc1Δ* cells expressing wild type copy of *SSC1* gene from a *URA* plasmid was transformed with either *SSC1* on a *CEN* plasmid or A, *A_yP_{Yl}* (*left panel*), *A_yP_I* (*middle panel*), *A_IP_{Yl}* (*right panel*) from a *CEN* pRS413 plasmid driven by *GPD* promoter. B, *A_{Hs}P_{Hs}* (*left panel*), *A_{Hs}P_I* (*middle panel*), *A_IP_{Hs}* (*right panel*) from a 2μ pRS423 plasmid driven by *TEF* promoter. The cells were streaked on media containing 5-fluoroorotic acid and grown at 30 °C for 3 days. The empty vector was used as a negative control.

Supplemental TABLE S1:**Plasmids used in this study**

| Plasmid name | Expressed protein | Leader sequence | Vector | Host Organism used | Restriction sites |
|---|---|-----------------|-------------------|---------------------|-------------------|
| pRS314-SSC1 | Ssc1 | Ssc1 | pRS314 | <i>S.cerevisiae</i> | PstI/ BamHI |
| pRS313-SSC3 | Ssc3 | Ssc3 | pRS313 | <i>S.cerevisiae</i> | HindIII/BamHI |
| pRS423-SSC3 | Ssc3 | Ssc1 | TEF/GPD pRS423 | <i>S.cerevisiae</i> | BamHI/XhoI |
| pRS423- A _I P ₃ | A _I P ₃ | Ssc1 | TEF/GPD pRS423 | <i>S.cerevisiae</i> | BamHI/XhoI |
| pRS423- A ₃ P ₁ | A ₃ P ₁ | Ssc1 | TEF/GPD pRS423 | <i>S.cerevisiae</i> | BamHI/XhoI |
| pRS423-A _{Hs} P _{Hs} | A _{Hs} P _{Hs} | Ssc1 | TEF pRS423 | <i>S.cerevisiae</i> | BamHI/XhoI |
| pRS423- A _I P _{Hs} | A _I P _{Hs} | Ssc1 | TEF pRS423 | <i>S.cerevisiae</i> | BamHI/XhoI |
| pRS423- A _{Hs} P _I | A _{Hs} P _I | Ssc1 | TEF pRS423 | <i>S.cerevisiae</i> | BamHI/XhoI |
| pRS413- A _{Yl} P _{Yl} | A _{Yl} P _{Yl} | Ssc1 | GPD pRS413 | <i>S.cerevisiae</i> | BamHI/EcoRI |
| pRS413- A _I P _{Yl} | A _I P _{Yl} | Ssc1 | GPD pRS413 | <i>S.cerevisiae</i> | BamHI/EcoRI |
| pRS413- A _{Yl} P _I | A _{Yl} P _I | Ssc1 | GPD pRS413 | <i>S.cerevisiae</i> | BamHI/EcoRI |
| pRS314-ssc1-2 | Ssc1-2 | Ssc1 | pRS314 | <i>S.cerevisiae</i> | PstI/ BamHI |
| pRSFDuet-1-Ssc1 | Ssc1(His ₆) | - | pRSFDuet-1 | <i>E. coli</i> BL21 | NdeI/XhoI |
| pRSFDuet-1-Ssc3 | Ssc3(His ₆) | - | pRSFDuet-1 | <i>E. coli</i> BL21 | NdeI/XhoI |
| pRSFDuet-1- Ssc3 ₅₅₈ | Ssc3(1-558) (His ₆) | - | pRSFDuet-1 | <i>E. coli</i> BL21 | NdeI/XhoI |
| pRSFDuet-1- Ssc3 ₅₂₈ | Ssc3 (1-528) (His ₆) | - | pRSFDuet-1 | <i>E. coli</i> BL21 | NdeI/XhoI |
| pET-3a-SBD _{Ssc1} | SBD _{Ssc1} (His ₆) | - | pET-3a | <i>E. coli</i> BL21 | NdeI/ BamHI |
| pET-21d-SBD _{Ssc3} | SBD _{Ssc3} (His ₆) | - | pET-21d | <i>E. coli</i> BL21 | NcoI/XhoI |
| pET-3a-SBD _{Ssc1-} (ABCD) _{Ssc3} | SBD _{Ssc1-} (ABCD) _{Ssc3} (His ₆) | - | pET-3a | <i>E. coli</i> BL21 | NdeI/ BamHI |
| pET-3a-SBD _{Ssc1-} (A) _{Ssc3} | SBD _{Ssc1-} (A) _{Ssc3} (His ₆) | - | pET-3a | <i>E. coli</i> BL21 | NdeI/ BamHI |
| pET-3a-SBD _{Ssc1-} (B) _{Ssc3} | SBD _{Ssc1-} (B) _{Ssc3} (His ₆) | - | pET-3a | <i>E. coli</i> BL21 | NdeI/ BamHI |
| pET-3a-SBD _{Ssc1-} (C) _{Ssc3} | SBD _{Ssc1-} (C) _{Ssc3} (His ₆) | - | pET-3a | <i>E. coli</i> BL21 | NdeI/ BamHI |
| pET-3a-SBD _{Ssc1-} (D) _{Ssc3} | SBD _{Ssc1-} (D) _{Ssc3} (His ₆) | - | pET-3a | <i>E. coli</i> BL21 | NdeI/ BamHI |
| pET-3a-SBD _{Ssc3-} (D) _{Ssc1} | SBD _{Ssc3-} (D) _{Ssc1} (His ₆) | - | pET-3a | <i>E. coli</i> BL21 | NdeI/ BamHI |
| pRSFDuet-1-NBD _{Ssc1} | NBD _{Ssc1} (His ₆) | - | pRSFDuet-1 | <i>E. coli</i> BL21 | NdeI/XhoI |
| pRSFDuet-1-NBD _{Ssc3} | NBD _{Ssc3} (His ₆) | - | pRSFDuet-1 | <i>E. coli</i> BL21 | NdeI/XhoI |
| pRSFDuet-1- Ssc1- V28IQ29PG30DS31A | Ssc1- V28IQ29PG30DS31A(His ₆) | - | pRSFDuet-1 | <i>E. coli</i> BL21 | NdeI/XhoI |
| pRSFDuet-1- Ssc1- | Ssc1- | - | pRSFDuet-1 | <i>E. coli</i> BL21 | NdeI/XhoI |

| | | | | | |
|---------------------------------------|---|---|------------|---------------------|------------|
| I80EA86SV88IP90S | I80EA86SV88I P90S (His ₆) | | | | |
| pRSFDuet-1- Ssc1-G135NQ136R | Ssc1-G135NQ136R(His ₆) | - | pRSFDuet-1 | <i>E. coli</i> BL21 | NdeI/XhoI |
| pRSFDuet-1- Ssc1-G160AP162S | Ssc1-G160AP162S (His ₆) | - | pRSFDuet-1 | <i>E. coli</i> BL21 | NdeI/XhoI |
| pRSFDuet-1- Ssc1-S214P | Ssc1-S214P (His ₆) | - | pRSFDuet-1 | <i>E. coli</i> BL21 | NdeI/XhoI |
| pRSFDuet-1- Ssc1-V238I | Ssc1-V238I (His ₆) | - | pRSFDuet-1 | <i>E. coli</i> BL21 | NdeI/XhoI |
| pRSFDuet-1- Ssc1-S314A | Ssc1-S314A (His ₆) | - | pRSFDuet-1 | <i>E. coli</i> BL21 | NdeI/XhoI |
| pRSFDuet-1- Ssc1-N320RK322P | Ssc1-N320RK322P (His ₆) | - | pRSFDuet-1 | <i>E. coli</i> BL21 | NdeI/XhoI |
| pRSFDuet-1- Ssc1-A326VF328LT330NL331I | Ssc1-A326VF328LT330NL331I (His ₆) | - | pRSFDuet-1 | <i>E. coli</i> BL21 | NdeI/XhoI |
| pRSFDuet-1- Ssc1-V336IK337D | Ssc1-V336IK337D (His ₆) | - | pRSFDuet-1 | <i>E. coli</i> BL21 | NdeI/XhoI |
| pRSFDuet-1- Ssc1-G351RL352IS353TT354A | Ssc1-G351RL352IS353TT354A (His ₆) | - | pRSFDuet-1 | <i>E. coli</i> BL21 | NdeI/XhoI |
| pRSFDuet-1- Ssc1-S378K | Ssc1-S378K (His ₆) | - | pRSFDuet-1 | <i>E. coli</i> BL21 | NdeI/XhoI |
| pRSFDuet-1- Ssc1-P384A | Ssc1-P384A (His ₆) | - | pRSFDuet-1 | <i>E. coli</i> BL21 | NdeI/XhoI |
| pRSFDuet-1- Ssc1-I396LV400IG402A | Ssc1-I396LV400IG402A (His ₆) | - | pRSFDuet-1 | <i>E. coli</i> BL21 | NdeI/XhoI |
| pRSFDuet-1- Ssc3-A157GS159P | Ssc3-A157GS159P (His ₆) | - | pRSFDuet-1 | <i>E. coli</i> BL21 | NdeI/XhoI |
| pRSFDuet-1-Hep1 | Hep1 | - | pRSFDuet-1 | <i>E. coli</i> BL21 | BamHI/SalI |
| pRSFDuet-1-Mge1 | Mge1(His ₆) | - | pRSFDuet-1 | <i>E. coli</i> BL21 | BamHI/SalI |
| pRSFDuet-1-Mdj1 | Mdj1(His ₆) | - | pRSFDuet-1 | <i>E. coli</i> BL21 | NdeI/XhoI |
| pET-3a-Pam18 | Pam18(His ₆) | - | pET-3a | <i>E. coli</i> C41 | NdeI/BamHI |
| pET-20b-Tim44 | Tim44 (TEV cleavable His ₆) | - | pET-20b | <i>E. coli</i> BL21 | BamHI/XhoI |

Supplemental TABLE S2:

S. cerevisiae strains used in this study

| Strain | Genotype | Source |
|--|---|-------------------------|
| PJ53-52C | (<i>trp1-1 ura3-1 leu2-3, 112 his3-11, 15 ade2-1 can1-100 GAL2+ met2-Δ1 lys2-Δ2 ssc1ΔClai::LEU2 pRS316-SSC1</i>) | Voisine, C. et al. (41) |
| PJ53-52C CEN SSC3 | (<i>trp1-1 ura3-1 leu2-3, 112 his3-11, 15 ade2-1 can1-100 GAL2+ met2-Δ1 lys2-Δ2 ssc1ΔClai::LEU2 pRS316-SSC1 pRS313-SSC3</i>) | This study |
| PJ53-52C 2μ SSC3 | (<i>trp1-1 ura3-1 leu2-3, 112 his3-11, 15 ade2-1 can1-100 GAL2+ met2-Δ1 lys2-Δ2 ssc1ΔClai::LEU2 pRS316-SSC1 pRS423-SSC3</i>) | This study |
| PJ53-52C <i>A_IP₃</i> | (<i>trp1-1 ura3-1 leu2-3, 112 his3-11, 15 ade2-1 can1-100 GAL2+ met2-Δ1 lys2-Δ2 ssc1ΔClai::LEU2 pRS316-SSC1 pRS423- A_IP₃</i>) | This study |
| PJ53-52C <i>A₃P_I</i> | (<i>trp1-1 ura3-1 leu2-3, 112 his3-11, 15 ade2-1 can1-100 GAL2+ met2-Δ1 lys2-Δ2 ssc1ΔClai::LEU2 pRS316-SSC1 pRS423- A₃P_I</i>) | This study |
| <i>A_IP₃</i> | (<i>trp1-1 ura3-1 leu2-3, 112 his3-11, 15 ade2-1 can1-100 GAL2+ met2-Δ1 lys2-Δ2 ssc1ΔClai::LEU2 pRS423- A_IP₃</i>) | This study |
| PJ53-52C <i>A_{Hs}P_{Hs}</i> | (<i>trp1-1 ura3-1 leu2-3, 112 his3-11, 15 ade2-1 can1-100 GAL2+ met2-Δ1 lys2-Δ2 ssc1ΔClai::LEU2 pRS316-SSC1 pRS423- A_{Hs}P_{Hs}</i>) | This study |
| PJ53-52C <i>A_IP_{Hs}</i> | (<i>trp1-1 ura3-1 leu2-3, 112 his3-11, 15 ade2-1 can1-100 GAL2+ met2-Δ1 lys2-Δ2 ssc1ΔClai::LEU2 pRS316-SSC1 pRS423- A_IP_{Hs}</i>) | This study |
| PJ53-52C <i>A_{Hs}P_I</i> | (<i>trp1-1 ura3-1 leu2-3, 112 his3-11, 15 ade2-1 can1-100 GAL2+ met2-Δ1 lys2-Δ2 ssc1ΔClai::LEU2 pRS316-SSC1 pRS423- A_{Hs}P_I</i>) | This study |
| <i>A_IP_{Hs}</i> | (<i>trp1-1 ura3-1 leu2-3, 112 his3-11, 15 ade2-1 can1-100 GAL2+ met2-Δ1 lys2-Δ2 ssc1ΔClai::LEU2 pRS423- A_IP_{Hs}</i>) | This study |
| <i>A_{Hs}P_I</i> | (<i>trp1-1 ura3-1 leu2-3, 112 his3-11, 15 ade2-1 can1-100 GAL2+ met2-Δ1 lys2-Δ2 ssc1ΔClai::LEU2 pRS423- A_{Hs}P_I</i>) | This study |
| PJ53-52C <i>A_{Yl}P_{Yl}</i> | (<i>trp1-1 ura3-1 leu2-3, 112 his3-11, 15 ade2-1 can1-100 GAL2+ met2-Δ1 lys2-Δ2 ssc1ΔClai::LEU2 pRS316-SSC1 pRS413- A_{Yl}P_{Yl}</i>) | This study |
| PJ53-52C <i>A_IP_{Yl}</i> | (<i>trp1-1 ura3-1 leu2-3, 112 his3-11, 15 ade2-1 can1-100 GAL2+ met2-Δ1 lys2-Δ2 ssc1ΔClai::LEU2 pRS316-SSC1 pRS413- A_IP_{Yl}</i>) | This study |
| PJ53-52C <i>A_{Yl}P_I</i> | (<i>trp1-1 ura3-1 leu2-3, 112 his3-11, 15 ade2-1 can1-100 GAL2+ met2-Δ1 lys2-Δ2 ssc1ΔClai::LEU2 pRS316-SSC1 pRS413- A_{Yl}P_I</i>) | This study |
| <i>A_{Yl}P_{Yl}</i> | (<i>trp1-1 ura3-1 leu2-3, 112 his3-11, 15 ade2-1 can1-100 GAL2+ met2-Δ1 lys2-Δ2 ssc1ΔClai::LEU2 pRS413- A_{Yl}P_{Yl}</i>) | This study |
| <i>A_IP_{Yl}</i> | (<i>trp1-1 ura3-1 leu2-3, 112 his3-11, 15 ade2-1 can1-100 GAL2+ met2-Δ1 lys2-Δ2 ssc1ΔClai::LEU2 pRS413- A_IP_{Yl}</i>) | This study |
| <i>A_{Yl}P_I</i> | (<i>trp1-1 ura3-1 leu2-3, 112 his3-11, 15 ade2-1 can1-100 GAL2+ met2-Δ1 lys2-Δ2 ssc1ΔClai::LEU2 pRS413- A_{Yl}P_I</i>) | This study |
| PJ53-52C <i>ssc1-2</i> | (<i>trp1-1 ura3-1 leu2-3, 112 his3-11, 15 ade2-1 can1-100 GAL2+ met2-Δ1 lys2-Δ2 ssc1ΔClai::LEU2 pRS314-ssc1-2</i>) | Voisine, C. et al. (41) |
| <i>ssc1-2</i> 2μ SSC3 | (<i>trp1-1 ura3-1 leu2-3, 112 his3-11, 15 ade2-1 can1-100 GAL2+ met2-Δ1 lys2-Δ2 ssc1ΔClai::LEU2 pRS314-ssc1-2</i>) | This study |

| | | |
|---------------------|---|------------------------|
| | pRS423-Ssc3) | |
| BY4741 | <i>MATa his3Δ1 leu2Δ met15Δ ura3Δ</i> | <i>Open Biosystems</i> |
| BY4741 <i>ssc3Δ</i> | <i>MATa his3Δ1 leu2Δ met15Δ ura3Δ ssc3Δ::kanMX4</i> | <i>Open Biosystems</i> |

Supplemental TABLE S3:**Kinetic parameters for F-P5 binding with SBD_{Ssc1}, SBD_{Ssc3} and chimeric proteins.**

| Protein | K _d (μM) | R ² |
|---|---------------------|----------------|
| SBD _{Ssc1} | 0.264 ± 0.041 | 0.98 |
| SBD _{Ssc1} -(ABCD) _{Ssc3} | 22.724 ± 1.008 | 0.97 |
| SBD _{Ssc1} -(A) _{Ssc3} | 0.293 ± 0.031 | 0.99 |
| SBD _{Ssc1} -(B) _{Ssc3} | 0.351 ± 0.033 | 0.99 |
| SBD _{Ssc1} -(C) _{Ssc3} | 0.285 ± 0.032 | 0.98 |
| SBD _{Ssc1} -(D) _{Ssc3} | 20.782 ± 0.983 | 0.97 |
| SBD _{Ssc3} | 26.897 ± 2.639 | 0.97 |
| SBD _{Ssc3} -(D) _{Ssc1} | 0.911 ± 0.087 | 0.99 |

Supplemental TABLE S4:**Aggregation of various mtHsp70 proteins at 37 °C in bacterial system.**

| Protein | Aggregation at 37 °C |
|----------------------|-----------------------------|
| Ssc1 | |
| WT | - |
| V28IQ29PG30DS31A | - |
| I80EA86SV88IP90S | * |
| G135NQ136R | - |
| G160AP162S | ** |
| S214P | - |
| V238I | * |
| S314A | - |
| N320RK322P | - |
| A326VF328LT330NL331I | - |
| V336IK337D | - |
| G351RL352IS353TT354A | * |
| S378K | - |
| P384A | - |
| I396LV400IG402A | - |
| Ssc3 | |
| WT | ***** |
| A157GS159P | **** |

Subjective scoring is based on the amount of protein present in pellet (P) fraction upon solubility analysis at 37 °C in *E.coli*. Here (******) has been assigned to Ssc3 owing to its maximum tendency to aggregate, while others are assigned relative to Ssc3 based on their distribution in supernatant and pellet fraction upon solubility analysis. (-) sign indicates no aggregation under similar conditions.

Supplemental TABLE S5:

Growth complementation of *ssc1Δ* strain (*PJ53-52C*) with various Hsp70 constructs at indicated temperatures.

| Strain | Growth complementation at | | | |
|----------------|---------------------------|-------|-------|-------|
| | 24 °C | 30 °C | 34 °C | 37 °C |
| WT PJ53-52C | +++ | +++ | +++ | +++ |
| A_3P_3 | - | - | - | - |
| A_3P_1 | - | - | - | - |
| A_1P_3 | +++ | +++ | ++ | - |
| $A_{Yl}P_{Yl}$ | ++ | ++ | + | - |
| $A_{Yl}P_1$ | ++ | ++ | + | - |
| A_1P_{Yl} | +++ | +++ | +++ | +++ |
| $A_{Hs}P_{Hs}$ | - | - | - | - |
| $A_{Hs}P_1$ | + | + | + | - |
| A_1P_{Hs} | ++ | ++ | ++ | + |

Subjective scoring is based on temperature sensitive phenotype mentioned in Fig.8 from strongest (+++) to weakest (+). Minus (-) indicates lethal phenotype at indicated temperature.

**Primary Sequence That Determines the Functional Overlap between
Mitochondrial Heat Shock Protein 70 Ssc1 and Ssc3 of *Saccharomyces cerevisiae***
Gautam Pareek, Madhuja Samaddar and Patrick D'Silva

J. Biol. Chem. 2011, 286:19001-19013.
doi: 10.1074/jbc.M110.197434 originally published online April 7, 2011

Access the most updated version of this article at doi: [10.1074/jbc.M110.197434](https://doi.org/10.1074/jbc.M110.197434)

Alerts:

- [When this article is cited](#)
- [When a correction for this article is posted](#)

[Click here](#) to choose from all of JBC's e-mail alerts

Supplemental material:

<http://www.jbc.org/content/suppl/2011/04/07/M110.197434.DC1.html>

This article cites 56 references, 24 of which can be accessed free at
<http://www.jbc.org/content/286/21/19001.full.html#ref-list-1>